Rejas, M., Taberner, C., Pueyo, J. J., Giralt, S., Mata, M. P., María de Gibert, J. and Díaz del Río, V., 2015. Origin of carbonate concretions from mud mounds in the Gulf of Cadiz (SW Iberian Peninsula). *Boletín Geológico y Minero,* 126 (2-3): 553-574
ISSN: 0366-0176

Origin of carbonate concretions from mud mounds in the Gulf of Cadiz (SW Iberian Peninsula)

M. Rejas[(1)], C. Taberner[(2)], J. J. Pueyo[(3)], S. Giralt[(1)], M. P. Mata[(4)], J. María de Gibert[(3)] and V. Díaz del Río[(5)]

(1) Institute of Earth Sciences Jaume Almera, ICTJA-CSIC, Lluís Solé i Sabarís s/n, 08028 Barcelona, Spain.
mrejas@ictja.csic.es, sgiralt@ictja.csic.es
(2) Shell GS International NL, Carbonate Research, Integrated Geoscience Department.
Kesslerpark 1, 2288 GS Rijswijk (ZH), The Netherlands.
Conxita.Taberner@shell.com
(3) Facultat de Geologia. Universitat de Barcelona. C/ Martí i Franqués s/n, Barcelona, E-08028, Spain.
jjpueyo@ ub.edu
(4) Spanish Geological Survey (IGME), C/ Ríos Rosas, 23, Madrid, E-28003, Spain.
p.mata@igme.es
(5) Spanish Institute of Oceanography (IEO). Fuengirola, Málaga E-29640, Spain.
diazdelrio@ma.ieo.es

ABSTRACT

The Gulf of Cadiz displays a number of structures that are associated with fluid circulation (mud volcanoes, mud mounds and pockmarks).This area has been used as natural laboratory for the sedimentological, biological and biogeochemical studies of these environments. Analysis of the associated authigenic carbonates has been widely used as a proxy to yield insights into the circulation and chemical composition of these fluids. A study of carbonate concretions from the Ibérico, Cornide and Arcos mud mounds in the Diasom Field was undertaken to better understand the origin and type of fluids from which these concretions precipitated. The concretions display varying morphologies, some of which correspond to bioturbation traces. X-ray diffractions revealed that these carbonate concretions are mainly composed of dolomite, Fe-rich dolomite, high magnesium calcite (HMC) and ankerite. The $\delta^{13}C$ values of carbonate minerals ranged between -48.3 and-10.9 ‰ V-PDB, which suggests that the main processes involved in their genesis are organic matter oxidation, bacterial sulphate-reduction (BSR) and anaerobic methane oxidation (AOM). The origin of the methane is mainly thermogenic, and only few concretions yielded $\delta^{13}C$ values lower than -40 ‰ V-PDB, suggesting oxidation of microbial methane. Fluids involved in the carbonate precipitation are interpreted as being related to gas hydrate destabilisation ($\delta^{18}O_{fluid\text{-}V\text{-}SMOW}$ values higher than +2 ‰) and, to a lesser extent, modified seawater enriched in ^{18}O due to rock-water interaction. Nevertheless, the highest $\delta^{18}O_{fluid\text{-}V\text{-}SMOW}$ values suggest that the influence of other deep-seated fluids due to clay-mineral dehydration cannot be ruled out.

Key words: authigenic carbonates, gas hydrates, Gulf of Cadiz, methane, mud mounds.

Origen de las concreciones carbonatadas de los montículos de fango en el Golfo de Cádiz (SO Península Ibérica)

RESUMEN

El Golfo de Cádiz, que muestra una gran variedad de estructuras asociadas a circulación de fluidos (volcanes de fango, montículos de fango y pockmarks), es una de las zonas más importantes para el estudio sedimentológico, biológico y biogeoquímico de ese tipo de ambientes. El análisis de los carbonatos autigénicos asociados a los montículos y volcanes de fango se ha utilizado extensamente en el estudio de la circulación y la composición química de los fluidos. Se han estudiado concreciones carbonatadas en los montículos de fango del Complejo de chimeneas carbonatadas Diasom (montículos de fango Ibérico, Cornide y Arcos) con objeto de conocer la naturaleza y origen de los fluidos implicados en la precipitación de las mismas. Las concreciones carbonatadas muestran una gran variedad de morfologías y tamaños, así como abundantes trazas de bioturbación. Los datos obtenidos mediante DRX confirman que las concreciones están formadas principalmente por dolomita, dolomita ferruginosa, calcita con alto contenido en magnesio (HMC) y ankerita. Los valores de $\delta^{13}C$, entre -48,3 y -10,9 ‰ V-PDB, sugieren que los principales procesos implicados en su génesis

son la oxidación de la materia orgánica, la sulfato-reducción bacteriana (BSR), y la oxidación anaeróbica de metano (AOM). El origen del metano es principalmente termogénico y sólo algunas concreciones muestran valores de $\delta^{13}C$ inferiores a -40 ‰ V-PDB, indicando la oxidación de metano microbiano. Los fluidos implicados en la precipitación del carbonato están relacionados principalmente con la desestabilización de hidratos de gas (valores de $\delta^{18}O_{fluido\ V\text{-}SMOW}$ superiores a +2 ‰) y, en menor grado, con agua marina modificada por enriquecimiento en ^{18}O causado por interacción roca-agua. No es posible descartar, sin embargo, la influencia de otros fluidos profundos relacionados con deshidratación de arcillas si tenemos en cuenta los valores más altos de $\delta^{18}O_{fluido\ -V\text{-}SMOW.}$

Palabras clave: carbonatos autigénicos, hidratos de gas, Golfo de Cádiz, metano, montículos de fango.

VERSIÓN ABREVIADA EN CASTELLANO

Introducción y metodología

Los carbonatos autigénicos de las surgencias frías son buenos indicadores de circulación de fluidos (p.ej., metano profundo, fluidos asociados a la desestabilización de hidratos de gas) dentro de los sedimentos. Este tipo de carbonatos ha sido identificado en materiales con edades comprendidas entre el Devónico medio y la actualidad (Peckmann et al., 1999; Peckmann et al., 2001), y en diferentes ambientes geodinámicos, tanto en márgenes continentales pasivos (Formolo et al., 2004; Mazzini et al., 2004; Gontharet et al., 2007) como activos (Kulm et al., 1986; Brown and Westbrook, 1988; Greinert et al., 2001; Han et al., 2004). Al contrario de lo que sucede con otros indicadores de circulación de fluidos, como es el caso de las depresiones circulares o los volcanes de fango, tienen un alto grado de preservación y son, por tanto, abundantes en el registro geológico.

Los minerales esenciales que los forman son aragonito, calcita con bajo contenido en magnesio (LMC), calcita con alto contenido en magnesio (HMC), dolomita, dolomita ferruginosa y ankerita. Estos carbonatos muestran un amplio rango de $\delta^{13}C$ que oscila entre -60 ‰ V-PDB y +20 ‰ V-PDB. Esta variabilidad se debe a la presencia de: a) fuentes de CO_2 diversas, b) metano de distintos orígenes (termogénico o microbiano), y c) procesos bioquímicos variados como la sulfato reducción bacteriana (BSR), la oxidación anaeróbica de metano (AOM), la metanogénesis y la oxidación de materia orgánica (Greinert et al., 2001; Formolo et al., 2004; Han et al., 2004; Mazzini et al., 2004 y 2006; Teichert et al, 2005; Gontharet et al., 2007). Muestran frecuentemente valores positivos de $\delta^{18}O$, que indican la presencia de fluidos enriquecidos en ^{18}O, procedentes de la descomposición de hidratos de gas y de la deshidratación de minerales arcillosos (p.ej. de la transformación de esmectita a illita).

En este trabajo se han estudiado concreciones carbonatadas obtenidas durante las campañas Anastasya 2000 y Anastasya 2001 (Tabla 1) correspondientes a tres montículos de fango (Ibérico, Cornide y Arcos) situados en el Campo de Diasom (Golfo de Cádiz) (Figs. 1 y 2). Se ha utilizado microscopía convencional, catodoluminiscencia y microscopía electrónica de barrido (SEM) para su caracterización estructural, difracción de rayos-X y análisis de elementos mayores (Ca, Sr, Mg, Fe y Mn) para la identificación mineralógica, y análisis isotópico ($\delta^{13}C$, $\delta^{18}O$, $^{87}Sr/^{86}Sr$) para obtener información sobre los procesos biogeoquímicos implicados.

Descripción macroscópica y petrografía

Las concreciones carbonatadas de Diasom muestran un amplio rango de tamaños y morfologías y han sido clasificadas en tres grandes grupos: irregulares, cónicas y cilíndricas (Fig. 3). Las concreciones más abundantes son las irregulares, localizadas principalmente en los montículos Ibérico y Cornide (Fig. 3A y B). Las concreciones cilíndricas (Ibérico, Cornide y Arcos) (Fig. 3C) suelen tener una cavidad cilíndrica interna, frecuentemente vacía (Fig. 3D). Las concreciones cónicas (Fig. 3E) presentes principalmente en Arcos y Cornide, son las menos abundantes y se caracterizan por tener una cavidad interna cerrada por un extremo (Fig. 3F). Las concreciones muestran en su superficie gran cantidad de organismos epifáunicos, entre los que están presentes Cnidaria (Fig. 3A), Porífera (Fig. 3F), Bivalvia y Polychaeta (Fig. 3F). Se han observado estructuras de bioerosión asociadas a la actividad de esponjas Gastrochaenolites (Fig. 3G), Trypanites, Taulostrepsis y Entobia, y de poliquetos Meandropolydora (Fig. 3F y G). Estas estructuras de bioerosión se producen después de la exhumación de las concreciones y su posterior colonización por organismos epifáunicos. También se han observado trazas de bioturbación, siendo la más abundante el icnogénero Chondrites (Fig. 4C y D) junto con los icnogéneros Thalassinoides, Zoophycos, Arenicolites.

Las texturas de las concreciones son de tipo 'mudstone-packstone' con luminiscencia media de color naranja (Fig. 4B) aunque en algunos casos, debido al alto contenido en componentes detríticos (p. ej., mues-

tra 217 de Ibérico con más de 30 % de cuarzo, Tabla 2), también muestran texturas 'mudstone-packstone' (Fig. 4A). El contenido en bioclastos es mínimo y sólo se han identificado componentes de las familias Globigerinidae y Pulleniatinidae (Fig. 4A). De forma aislada, y sólo en algunas concreciones cónicas del montículo de fango Arcos, se han encontrado óxidos de Fe con texturas framboidales seudomórficas de pirita, de tamaños inferiores a 20 μm (Fig. 4E y F).

Mineralogía y composición química

El contenido en carbonato de las concreciones varía entre el 27 wt % (muestra 232 a.1) y el 98 wt % (muestra 291 c.3, Tabla 2). Las concreciones del montículo de fango Cornide son las que presentan contenidos más constantes de carbonato (en torno al 86 wt %).

Los principales minerales son dolomita, dolomita ferruginosa y calcita con alto contenido en magnesio (HMC), aunque en el montículo de fango Ibérico se han encontrado algunas muestras formadas por ankerita. La fracción detrítica está constituida principalmente por cuarzo y pequeñas cantidades de feldespatos.

La concentración de calcio es bastante constante en todas las muestras (26.2 wt % de CaO) (Tabla 3). El contenido en magnesio oscila entre 2.4 y 12.9 wt % de MgO, el de hierro entre 1.91 y 5.40 wt % de FeO y las concentraciones de estroncio y manganeso son inferiores a 0,15 wt % de SrO y 0.07 wt % de MnO, respectivamente.

Composición isotópica ($\delta^{13}C$, $\delta^{18}O$, $^{87}Sr/^{86}Sr$)

Las concreciones carbonatadas de Diasom presentan valores de $\delta^{13}C$ que oscilan entre -48.3 y -10.9 ‰ V-PDB, y de $\delta^{18}O$ entre +2.4 y +7.6 ‰ V-PDB (Tabla 3). El montículo Ibérico muestra valores de $\delta^{13}C$ entre -45.3 y -14.7 ‰ V-PDB para muestras de dolomita y de dolomita ferruginosa, y entre -36.7 y -32.5 ‰ V-PDB para la ankerita. Los valores de $\delta^{18}O$ oscilan entre +3.1 y +7.0 ‰ V-PDB para dolomitas y dolomitas ferruginosas, y entre +3.1 y + 8.9 ‰ V-PDB para la ankerita (Fig. 5). Las concreciones de Cornide (dolomita y dolomita ferruginosa) tienen $\delta^{13}C$ que varían de -48.3 a -14.4 ‰ V-PDB, y $\delta^{18}O$ entre +5.7 y +7.6 ‰ V-PDB. Las muestras de HMC del montículo Arcos son las que presentan los valores más altos en ^{13}C, que oscilan entre -29.3 y -10.9 ‰ V-PDB, y los valores más bajos de $\delta^{18}O$ (entre +2.2 y +3.6 ‰ V-PDB).

La relación $^{87}Sr/^{86}Sr$ muestra valores entre 0.70933, en una muestra de dolomita perteneciente al montículo de fango Cornide, y 0.70881, para una muestra de HMC del montículo de fango Arcos (Tabla 4).

Origen del metano implicado en la formación de las concreciones carbonatadas

La dispersión de los valores de $\delta^{13}C$ implica la existencia de diferentes fuentes de CO_2 durante la precipitación de los carbonatos. Las muestras de HMC del montículo Arcos, junto con las de dolomita y dolomita ferruginosa de los montículos Ibérico y Cornide, que presentan los valores más enriquecidos en ^{13}C, indican la contribución de CO_2 derivado de BSR y de oxidación de la materia orgánica. En cambio, los valores más empobrecidos en ^{13}C de Ibérico y Cornide reflejan la influencia de la oxidación anaeróbica de metano (AOM) asociada a BSR (Fig. 6).

El origen del metano implicado es principalmente termogénico ya que se observan valores de $\delta^{13}C$ superiores a -40 ‰ V-PDB. La presencia de metano termogénico en esta zona ha sido confirmada por medidas directas de gas realizadas por otros autores en volcanes de fango de la zona (Stadnitskaia et al., 2006; Nuzzo et al., 2009), y por el estudio de otros carbonatos autigénicos del Golfo de Cádiz (Díaz del Río et al., 2003; Magalhães, 2007; Magalhães et al., 2012; Vanneste et al., 2012). Sin embargo, no se puede descartar la presencia de metano microbiano ya que se encuentran valores inferiores a -40 ‰ V-PDB situados en la zona de indefinición isotópica entre metano microbiano y termogénico.

Origen de los fluidos implicados en la génesis de las concreciones

A partir de los valores de $\delta^{18}O_{V\text{-}PDB}$ de las concreciones y de la temperatura de precipitación se puede calcular el valor $\delta^{18}O_{V\text{-}SMOW}$ del fluido del que ha precipitado el carbonato en condiciones de equilibrio. Ya que no se dispone de un valor directo de temperatura en el momento de la precipitación, ni de inclusiones fluidas que permitieran calcularlo, se ha asumido el valor publicado de temperatura actual en dicha zona a esa profundidad, que es de 14°C (Gardner, 2001; Ambar et al., 2002; Díaz del Río et al., 2003; Hensen et al., 2007).

Las muestras de HMC y de ankerita (montículos de Arcos e Ibérico) muestran unos valores calculados de

$\delta^{18}O_{fluidoV\text{-}SMOW}$ que oscilan entre +0.9 y +2.9 ‰ y las muestras de dolomita y dolomita ferruginosa (Ibérico, Cornide y Arcos) entre +3.0 y +3.9 ‰ V-SMOW. Los valores más empobrecidos en ^{18}O indican la presencia de agua marina o fluidos de composición marina afectados por procesos de interacción roca-agua. Valores más altos de +1.5 ‰ V-SMOW pueden reflejar la contribución de fluidos generados por descomposición de hidratos de gas ya que, durante la formación de los mismos, el oxígeno se fracciona isotópicamente causando un enriquecimiento en ^{18}O estimado en +3.0 ± 0.1 ‰ V-SMOW. Otro proceso que puede generar fluidos acuosos enriquecidos en ^{18}O es la deshidratación de minerales arcillosos (transformación esmectita-illita) que dan lugar a fluidos con $\delta^{18}O_{fluido\ V\text{-}SMOW}$ superiores a +8 ‰ (Dählmann and de Lange, 2003; Gontharet et al., 2007; Hensen et al., 2007).

Formación de las concreciones carbonatadas en el Golfo de Cádiz

Las concreciones de los tres montículos de fango, Ibérico, Cornide y Arcos, se forman dentro de la zona de sulfato-reducción bacteriana (SRZ) caracterizada por la presencia de sulfato junto con materia orgánica y metano. Normalmente, en esta zona los minerales dominantes son aragonito y calcita con bajo contenido en Mg (LMC) debido a que el Mg^{2+} marino disponible se combina con el sulfato formando $MgSO_4$. En nuestro caso, sin embargo, la mineralogía dominante es dolomita y HMC ya que hay abundante Mg^{2+} libre debido a que el sulfato es consumido en el proceso de BSR y AOM. La presencia de metano en el sedimento se ve favorecida por la actividad bioturbadora de los organismos cuando el sedimento todavía no está consolidado. La bioturbación produce un aumento de la permeabilidad en el fango favoreciendo la redistribución de la materia orgánica y la circulación de metano, así como la de fluidos derivados de la desestabilización de los hidratos de gas o asociados a procesos de deshidratación de minerales arcillosos en profundidad.

Introduction

Evidence for the circulation of fluids (e.g., hydrocarbons, methane) through the sediments on the sea-floor has been provided by the presence of: a) circular depressions or "pockmarks" (Hovland *et al*., 1987; Mazzini *et al*., 2006; Gontharet *et al*., 2007), b) chemosymbiotic communities such as mussels, bivalves, tube worms, gastropods (e.g., Aharon, 1994; Cavagna *et al*., 1999), c) bacterial mats at the sediment-water interface (Boetius *et al*., 2000), and d) mud volcanoes, mud mounds and mud diapirism (e.g., Brown and Westbrook, 1988; Díaz del Río *et al*., 2003).

Mud volcanoes are produced by the eruption of mud triggered by the vertical circulation of hydrocarbon-rich fluids (Somoza *et al*., 2003). These structures are mainly symmetrical cone-shaped mounds with gentle slopes. Mud injections, hydrocarbons and mud-brecchia fragments may be observed on the slopes of the cone. Mud mounds are mud-accumulations on the sea-floor (Brown and Westbrook, 1988; Díaz del Río *et al*., 2003) with asymmetrical flanks and slopes up to 25° (Somoza *et al*., 2003). They are characterised by the presence of methane-related carbonates and the absence of mud-brecchia deposits.

The presence of hydrocarbon-derived cold-seep carbonates, crusts, slabs and concretions also provides ample evidence of fluid circulation (e.g., Greinert *et al*., 2001; Peckmann *et al*., 2001; Teichert *et al*., 2005; Naehr *et al*., 2007). These carbonates extend from the Middle Devonian to the Recent (Peckmann *et al*., 1999 and 2001). Today, cold-seep carbonate deposits are located in both active (e.g., the Costa Rica margin: Han *et al*., 2004; the Cascadia margin: Kulm *et al*., 1986; Greinert *et al*., 2001; the Barbados Ridge: Brown and Westbrook, 1988) and passive continental margin settings (e.g., the Mediterranean Sea: Gontharet *et al*., 2007; Gulf of Mexico: Formolo *et al*., 2004; the Black Sea: Mazzini *et al*., 2004) as well as around submarine mud volcanoes and mud mounds (e.g., Aloisi *et al*., 2000).

One of the main features of these authigenic carbonates is that they are well preserved in the sediment, enabling us to detect ancient seeps. In contrast, pockmarks and mud volcanoes are poorly preserved (Cavagna *et al*., 1999). Some authors use the presence of chemo-symbiotic fauna as the best marker of ancient cold seeps (e.g., Campbell and Bottjer, 1993; Kelly *et al*., 1995; Shapiro and Fricke, 2002; Conti *et al*., 2004; Gill *et al*., 2005). To interpret ancient seeps, Cavagna *et al*. (1999) undertook a review of diagnostic features such as the presence of: a) an irregular complex of fractures and cavities such as fluid-flow conduits (Kauffman *et al*., 1996), b) microbial fabrics such as stromatolites, thrombolites, laminated crusts and clotted peloids (Cavagna *et al*., 1999; Campbell *et al*., 2002; Greinert *et al*., 2002; Shapiro, 2004; Peckmann and Thiel, 2004; Campbell, 2006), c) biomarker compounds such as isoprene-based archaeallipids and hopanoids (Thiel *et al*., 1999; Burhan *et al*., 2002; Peckmann *et al*., 2002 and 2004; Peckmann and

Thiel, 2004; Stadnitskaia *et al*., 2007 and 2008), d) paragenetic sequences and porosities filled with different minerals (i.e., calcite, aragonite, barite, pyrite) (Clari *et al*., 1994; Terzi *et al*., 1994; Vanneste *et al*., 2012), and e) a limited lateral extent of the authigenic carbonates (de Boever *et al*., 2006). Most of these features are also observed in the recent cold-seep carbonates.

Precipitation of cold-seep carbonates is induced by anaerobic methane oxidation (AOM) linked to sulphate reduction (e.g., Ritger *et al*., 1987; Mazzini *et al*., 2004). AOM is mediated by a consortium of methanotrophic archaea and sulphate-reducing bacteria (Boetius *et al*., 2000; Michaelis *et al*., 2002) following the overall reaction:

$$CH_4+SO_4^{2-} \rightarrow HCO^-_3+HS^-+H_2O$$

AOM produces an increase in alkalinity in pore water, which favours carbonate precipitation (Berner, 1980). The origin of methane maybe either thermogenic, i.e. owing to thermal decomposition of organic matter (Schoell, 1980) in depths exceeding 2 km when the temperature reaches values higher than 100 °C, or microbial, i.e. associated with bacterial activity (Claypool and Kaplan, 1974; Irwin *et al*., 1977).

Cold-seep carbonates show a wide range of $\delta^{13}C$ values, from -60 ‰ V-PDB up to +20 ‰ V-PDB. This range provides evidence of multiple carbon sources and different biogeochemical processes involved in carbonate precipitation: bacterial sulphate-reduction, anaerobic methane oxidation, methanogenesis and oxidation of organic matter (Greinert *et al*., 2001; Formolo *et al*., 2004; Han *et al*., 2004; Mazzini *et al*., 2004; Gontharet *et al*., 2007; Teichert *et al*, 2005). Moreover, cold-seep carbonates often show anomalously positive $\delta^{18}O_{V\text{-}PDB}$, suggesting the presence of ^{18}O-enriched formation waters, gas hydrate decomposition fluids (e.g., Aloisi *et al*., 2000; Naehr *et al*., 2007) or clay dehydration water (smectite to illite transformation, Gontharet *et al*., 2007; Hensen *et al*., 2007; Haffert *et al*., 2012; Mata *et al*., 2012; Chao *et al*., 2013). Depleted values of $\delta^{18}O$ indicate the influence of meteoric water (Naehr *et al*., 2007). All these data suggest that cold-seep carbonate formation is mainly controlled by local features (i.e., methane flux, presence of gas hydrates) and not by the overall geological setting (Cavagna *et al*., 1999; Naehr *et al*., 2007).

As regards methane-related carbonates, the Gulf of Cadiz has become an important benchmark for the formation of these methane-related carbonates. The growing interest in the Gulf of Cadiz is reflected in the number of national and international research projects and cruises carried out in the area (e.g.de Haas *et al*. 2005, R.V. Pelagia cruise M2005; Mienis *et al*. 2004, R.V Pelagia cruise M2004; 2000 and 2001 Anastasya cruises).

Our paper presents the results of the study of recent carbonate concretions collected in the Diasom Field (Gulf of Cadiz) and provides new textural and isotopic data on the concretions. The main aims are to determine the origin of methane (thermogenic "vs." microbial) and to unravel new data on biogeochemical processes involved in the formation of these concretions.

Geological setting

The Gulf of Cadiz is located westwards of the Strait of Gibraltar and is bounded by the Iberian Peninsula and Morocco, between 9° W-6° 45 W and 34° N-37° 15 N (Fig. 1). The area has been affected by different tectonic events that have generated a complex structure due to the interaction of the Iberian rifted margin, the Arc of Gibraltar, and the convergence of the African and Eurasian plates (Banda *et al*., 1995; Gràcia *et al*., 2003). The morphology and structural history of the Gulf of Cadiz is still under discussion (Sartori *et al*., 1994; Maldonado *et al*., 1999; van Rensbergen, 2005) as most the studies have been done on the shelf and few studies offshore (Flinch, 1996; Tortella *et al*., 1997; González *et al*., 1998; Lobo *et al*., 2000). However, some recent studies (Gràcia *et al*., 2003; Iribarren *et al*., 2007) have yielded significant data on the outer part of the Gulf of Cadiz.

One of the main geological units is of late Miocene age, and is known under a variety of names: seismically chaotic body (Torelli *et al*., 1997), the Guadalquivir allochthonous unit (Berástegui *et al*., 1998), the olistostrome unit (Maldonado *et al*., 1999) or "Olistostrome" complex (Medialdea *et al*., 2004). This unit covers the central part of the Gulf of Cadiz and is composed of reworked sediments, mostly Triassic evaporites and Jurassic to Middle Miocene sediments (Iribarren *et al*., 2007). It was definitely emplaced in its current location in the Late Miocene (Torrelli *et al*., 1997; Medialdea *et al*., 2004; Fernández-Puga *et al*., 2007). Mud volcanoes, diapiric structures and authigenic carbonates associated with methane fluxes are common in the upper part of this complex (e.g., Díaz del Río *et al*., 2003; Fernández-Puga *et al*., 2007).

The Diasom Field is located close to the frontal wedge of the Olistostrome unit, which forms part of the Guadalquivir Diapiric Ridge (GDR) where several mud mounds have been discovered (Fig. 2). Carbonate concretions for study were obtained from

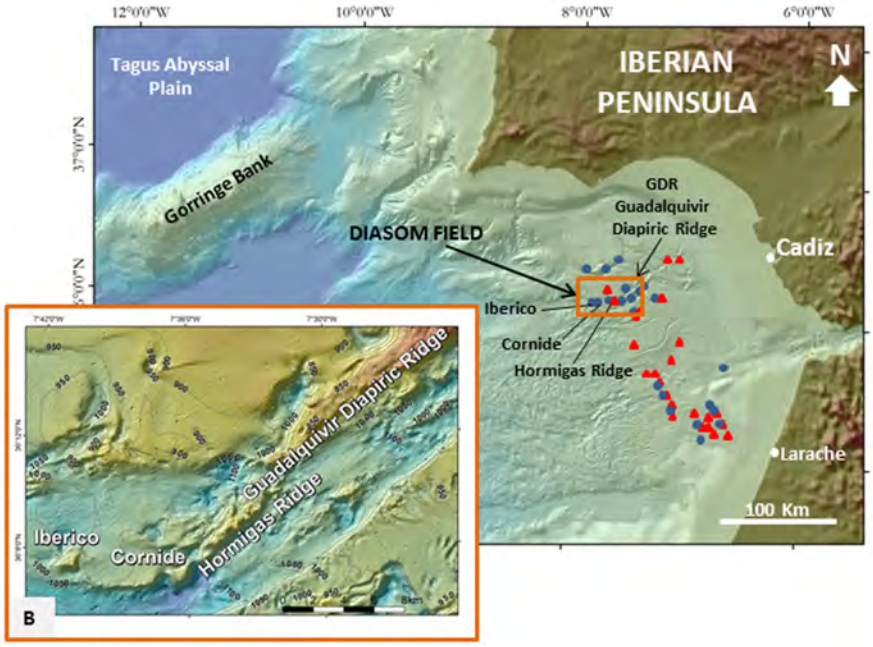

Figure 1. Map showing the situation of the mud volcanoes and mud mounds discovered in the Gulf of Cadiz. Red triangles: mud volcanoes, blue circles: mud mounds. B: Detail of the Diasom Field showing the three studied mud mounds: Ibérico, Cornide and Arcos (located at the Hormigas Ridge).

Figura 1. *Mapa mostrando la situación de los volcanes y montículos de fango descubiertos en el Golfo de Cádiz. Triángulos rojos: volcanes de fango, círculos azules: montículos de fango. B: Detalle del Campo Diasom mostrando los tres montículos de fango estudiados: Ibérico, Cornide y Arcos (localizado en la cresta Hormigas).*

the Ibérico, Cornide and Arcos mud mounds located in the Diasom Field. The Ibérico mound was one of the first places in the Gulf of Cadiz where authigenic carbonates were dredged (Díaz del Río *et al.*, 2001 and2003). The Ibérico mound (36° 6.96 N, 7° 41.08 W) rises 165 m above the surrounding seafloor at 870 mbsl (metres below sea level). The Cornide mound (36° 6.96 N, 7° 36.30 W) has the highest peak in the Diasom Field, rising 230 m above the seafloor at 950 mbsl. Seafloor observations show a large amount of carbonate concretions and carbonate slabs at the top of the Cornide mound (Díaz del Río *et al.*, 2003). The Arcos mound (36° 9.17 N, 7° 33.35 W) is located on the Hormigas Ridge, and attains a maximum height of 200 m at 850 mbsl.

Materials and methods

Sampling

Samples were retrieved from the seafloor with a rectangular benthic-type dredge during the Anastasya cruises in 2000 and 2001 (Table 1). The sampling depth ranged from 850 to 1,100 mbsl, and each dredge covered an area between 300 and 500 m.

Carbonate mineralogy, geochemical composition and petrography

A total of 40 carbonate samples were studied. These were photographed and described macroscopically. All the samples were labelled, microdrilled for XRD and analysed for major element and isotopic compositions. Polished thin sections (30 μm thick) were obtained from cut slabs and examined using standard optical microscopy, cathodoluminescence and scanning electron microscopy (SEM). Optical microscopy was performed with a Nikon Axiophot petrographic microscope and microphotographs were obtained using a DXC-S500 Sony CCD camera. Optical cathodoluminescence microscopy was carried out using a Nikon Labophot microscope equipped with a Cold Cathodoluminescence Technosyn 8200 MK-II unit. SEM observations were performed without conductive coating in a Quanta 200 SEI microscope working in low vacuum mode (~0.5 mbar).

The bulk mineralogical composition was determined using a Bruker D-5005 X-ray diffractometer at the Jaume Almera Institute of Earth Sciences (ICTJA-CSIC). The weight percent (wt %) of carbonate minerals was semi-quantitatively determined using the Reference Intensity Ratio (RIR) method (Chung, 1974).

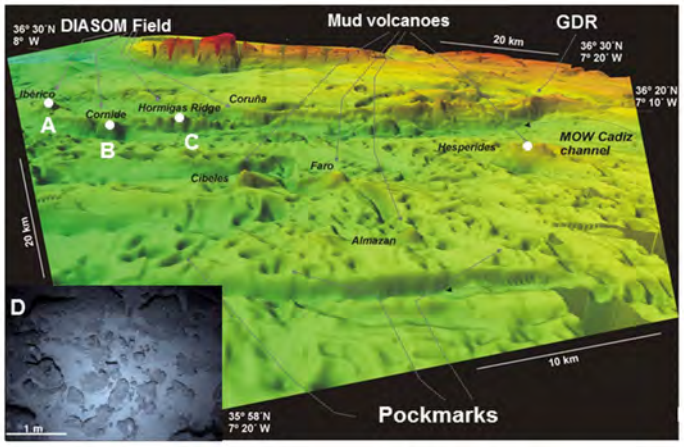

Figure 2. 3D bathymetric image of the study area in the Gulf of Cadiz. The area corresponds to a sector of the Guadalquivir Diapiric Ridge (GDR) where the Diasom Field is located. A: Ibérico mud mound, B: Cornide mud mound, C: Arcos mud mound (modified from Hernández-Molina *et al.,* 2003). Photo D shows a seafloor image from the Diasom Field. There is a large amount of carbonate concretions, showing a wide range of morphologies and sizes.
Figura 2. *Imagen batimétrica 3D del área de estudio en el Golfo de Cádiz. El área corresponde a un sector del Guadalquivir Diapiric Ridge (GDR) donde se localiza el Campo Diasom. A: montículo de fango Ibérico, B: montículo de fango Cornide, C: montículo de fango Arcos (modificada de Hernández-Molina et al., 2003). La fotografía D muestra una imagen del fondo marino en el Campo de Diasom. Se puede observar una gran cantidad de concreciones carbonatadas que muestran un amplio rango de morfologías y tamaños.*

Displacement of the (104) d-spacing was used to calculate the mol % $MgCO_3$ content (Goldsmith *et al.*, 1961). Calcite with less than 4 mol % $MgCO_3$ was considered as low magnesium calcite (LMC), and between 4 and 20 mol % $MgCO_3$ as high magnesium calcite (HMC) (Burton and Walter, 1987).

Major elements (calcium, strontium, manganese, iron, silicon and magnesium) of nine selected monomineralic samples were quantified with a Perkin-Elmer Elan 6000 ICP-MS spectrometer at the Scientific and Technological Centres of the University of Barcelona (CCiTUB). The values were expressed as wt % of oxides and, the precision (expressed as 2σ) was around 2%, depending on the element. In order to determine whether the d-spacing (104) drift of dolomite was due to an excess of Ca^{2+} or to the presence of Fe^{2+} in the crystal lattice, selected bulk samples composed of only dolomite or calcite with tiny amounts of siliciclastic minerals and non iron-oxides were analysed to quantify the mol % $FeCO_3$.

Oxygen and carbon isotopic analysis

$\delta^{13}C$ and $\delta^{18}O$ were also measured at the CCiTUB using a Finnigan Mat-252 mass spectrometer on-line connected to a Kiel unit. HMC samples were reacted with ortho-phosphoric acid at 70 °C for 3 minutes and dolomite samples for 15 minutes. The results are reported in delta notation (δ) relative to the Vienna Pee Dee Belemnite (V-PDB) international standard. Replicate analyses showed that precision was better than ± 0.02 ‰ for carbon and ± 0.06 ‰ for oxygen. The reference standard was NBS-19 ($\delta^{13}C_{V\text{-}PDB}$= +1.95 ‰ and $\delta^{18}O_{V\text{-}PDB}$= -2.20 ‰). The $\delta^{18}O$ values for dolomite concretions were recalculated using the fractionation factor (at 70°C, =1.01065) proposed by Rosenbaum and Sheppard (1986).

$^{87}Sr/^{86}Sr$ isotopic ratio

The $^{87}Sr/^{86}Sr$ isotopic ratio was determined on bulk samples using a Finnigan MAT-262 thermal ionisation-mass spectrometer. Samples were treated following the procedure described by Pin and Bassin (1992).The analytical data were corrected by the linear mass fractionation law taking as a constant the ratio $^{86}Sr/^{88}Sr$=0.1194 (Steiger and Jäger, 1977). The $^{87}Sr/^{86}Sr$ values were expressed with respect to the standard NBS-987 ($^{87}Sr/^{86}Sr$=0.710248), yielding a standard deviation of ± 0.000016 (1 σ).

Cruise	Dredge	Region of Diasom Field	Latitude start-dredge (°N)	Longitude start-dredge (°W)	Latitude end-dredge (°N)	Longitude end-dredge (°W)	samples
ANASTASYA 2000	DA-10	**IBÉRICO**	36° 07.00′	7 °41.50′	36°07.48′	7 °40.77′	214 to 227, 265, 266, 267, 291, 292
ANASTASYA 2001	DA-01	**CORNIDE**	36°06.96′	7°36.31′	36°07.08′	7°36.07′	200
ANASTASYA 2001	DA-02	**CORNIDE**	36°06.48′	7°36.93′	36°07.28′	7°36.55′	201, 202, 203, 204, 239 to 260
ANASTASYA 2001	DA-18	**ARCOS**	36°09.29′	7°32.89′	36°09.48′	7°33.47′	230 to 238, 277 to 286, 293

Table 1. Summary of the carbonate concretions dredged from the Diasom Field. Initial and final positions for each dredge are shown.
Tabla 1. *Resumen de las concreciones carbonatadas dragadas del Campo Diasom. Para cada draga se indican las posiciones inicial y final.*

Results

Macroscopic description and petrography

Since carbonate concretions from the Ibérico, Cornide and Arcos mud mounds vary in size and morphology they were classified into three morphological groups: irregular, conical and cylindrical.

Irregular concretions were mainly sampled in the Ibérico and Cornide mounds and are the most common morphotypes. They are characterized by irregular geometries of varying sizes (10 to 55 cm in length) and commonly by a ramdomly-oriented inner cylindrical cavity filled with carbonate-cemented sediment (Fig. 3A and B).

Cylindrical concretions sampled in the Ibérico, Cornide and Arcos mud mounds range from 10 to 45 cm in length (Fig. 3C and D). These concretions also show an inner elongated cavity parallel to the outer concretion surface. The cavity opens at both ends and is usually empty (Fig. 3D). In some concretions, the central channel forks into two cylindrical cavities.

Conical concretions (mainly dredged in the Arcos and Cornide mounds) range from 15 to 30 cm in length and display a single internal empty cavity with a dead end (Fig. 3E and F).

The concretion surface is mainly grey, but also light orange, brownish-red and dark brown (Fig. 3). A wide range of epifaunal organisms *Cnidaria* (Fig. 3A)*, Porifera* (Fig. 3F), *Bivalvia* and *Polychaeta* (Fig. 3F) are attached to the concretion.

Sponge bioerosion structures such as *Gastrochaenolites* (Fig. 3G)*, Trypanites, Taulostrepsis, Entobia*, and polychaete bioerosion marks (*Meandropolydora*) (Fig. 3F and G) are common. These structures were colonised by epifaunic organisms after the exhumation of the concretions. Bioturbation types (ichnogenus) are also present. The most common structure in the irregular concretions of the Cornide mound is *Chondrites* (Fig. 4C and D), but *Thalassinoides*, *Zoophycos*, *Arenicolites* were also identified. Moreover, a large number of undefined burrows (Fig. 4B) were also found, mainly in the Ibérico and Cornide mounds.

Overall, the concretions display mudstone-wackestone textures with a medium-bright orange luminescence (Fig. 4A and B). Some samples show a wackestone-packstone texture, with relatively large amounts of detrital grains, e.g. sample 217 from the Ibérico mound with more than 30% quartz (Fig. 4A). Bioclasts, including planktonic foraminifera *Globigerinidae* and *Pulleniatinidae* were rarely observed (Fig. 4A).

The lack of porosity is a distinctive feature of the concretions in the Diasom Field. Only small amounts of intraparticle porosity are observed in planktonic foraminifera and in the bioturbation fillings. Fe-oxides with framboidal texture were found in some conical concretions from the Arcos mound (Fig. 4E and F). These framboids have a spherical shape and are less than 20 μm in size.

Mineralogy and chemical composition

The carbonate content of concretions range from 27 wt % (sample 232 a.1 from the Arcos mound) up to 98 wt % (samples 291 c.3 from the Ibérico mound and 241 d.2 from the Cornide mound; Table 2). The concretions from the Cornide mound have a relatively

Figure 3. Morphologies observed in samples from the Ibérico, Cornide and Arcos mounds. A) Irregular concretion with nodular protuberances in the central part. Serpulids, corals (white arrow) and other epifaunic organisms placed on the concretion surface, Ibérico mound, sample 215; B) Irregular concretion with many burrow cavities (white arrow) filled by carbonate, Cornide mound, sample 241; C) Cylindrical concretion with an internal cavity (as shown in D, hidden in the photo), Ibérico mound, sample 214; D) Longitudinal section of a cylindrical concretion showing the internal cavity, Arcos mound, sample 231; E) Conical concretion with an empty cavity (hidden in the photo) and a single open end (see top of concretion), Arcos mound, sample 279; F) Empty cavity of a conical concretion. Serpulids, and sponges are partially filling the cavity (white arrow), Arcos mound, sample 235; G) Detail of *Meandropolydora*, polychaete boring activity (white arrow), Ibérico mound, sample 215; and H) *Gastrochaenolites* ichnogenus (bivalve) boring activity (white arrows) covered by serpulids (red arrow) and sponge overgrowths, Cornide mound, sample 260.

Figura 3. *Resumen de las diferentes morfologías observadas en las muestras de los montículos de fango Ibérico, Cornide y Arcos. A) Detalle de una concreción de morfología irregular con protuberancias nodulares en la parte central. Serpúlidos, corales (flecha blanca) y otros organismos epifáunicos situados en la superficie de la concreción, montículo Ibérico, muestra 215; B) Concreción irregular que muestra una intensa bioturbación (flecha blanca) rellena de carbonato, montículo Cornide, muestra 241; C) Concreción cilíndrica con cavidad interna oculta (ver imagen D), montículo Ibérico, muestra 214; D) Sección longitudinal de una concreción cilíndrica mostrando la cavidad interna, montículo de Arcos, muestra 231; E) Concreción de tipo cónico. La cavidad está vacía y muestra un orificio en su parte alta, montículo Arcos, muestra 279; F) Detalle de la cavidad característica de la concreciones cónicas. Se observan serpúlidos y esponjas llenando parcialmente la cavidad (flecha blanca), montículo Arcos, muestra 235; G) Detalle de la actividad perforadora de poliquetos (flecha blanca) del icnogénero Meandropolydora, montículo Ibérico, muestra 215; y H) Actividad perforante de bivalvos del icnogénero Gastrochaenolites (flechas blancas) cubierta por serpúlidos (flecha roja) y sobrecrecimientos de esponjas, montículo Cornide, muestra 260.*

high carbonate content (maximum: 98 wt %, minimum: 80 wt %, average: 88 ± 3.5 wt %), whereas the Ibérico and Arcos concretions show a considerable variability (Ibérico, maximum: 98 wt %, minimum: 28 wt %, average: 70 ± 17 wt %, Arcos, maximum: 94 wt %, minimum: 27 wt %, average: 66 ± 15.7 wt %).

The most abundant minerals in the concretions are dolomite, Fe-bearing dolomite and high magnesium calcite (HMC). The HMC occurs mainly in the Arcos concretions (samples 234, 279, 280, 281, 282, 284; Table 2), and also in two samples (samples 219 and 291; Table 2) composed mainly of ankerite from

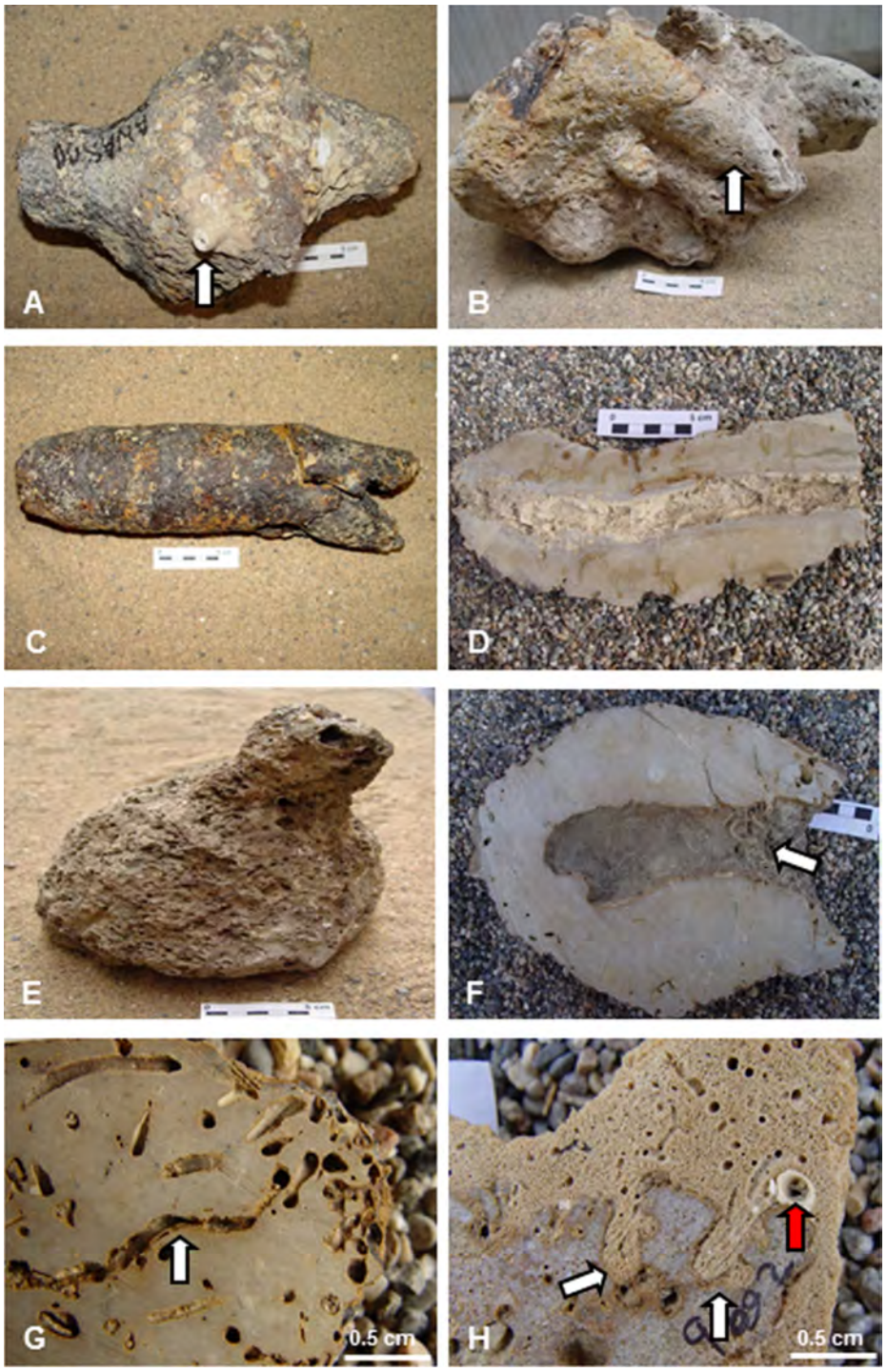

the Ibérico mound. The detrital content of the concretions is mainly composed of quartz, Fe-oxides and small amounts of feldspars (Table 2).

The calcium concentration (expressed as CaO) is very similar in all samples (the average value is 26.2 ± 2.1 wt %) (Table 3). The magnesium content (as MgO) ranges between 2.4 and 12.9 wt % with an average value of 8.1 % ± 3.9 wt %. The highest magnesium content is found in the Cornide concretions. The mean strontium (as SrO) and manganese (as MnO) concentrations are 0.1 ± 0.03 wt % and 0.06 ± 0.01 wt %), respectively, whereas the iron content (expressed as FeO) oscillates between 1.91 % and 5.40 % (average: 3.7 ± 1.2 wt %).

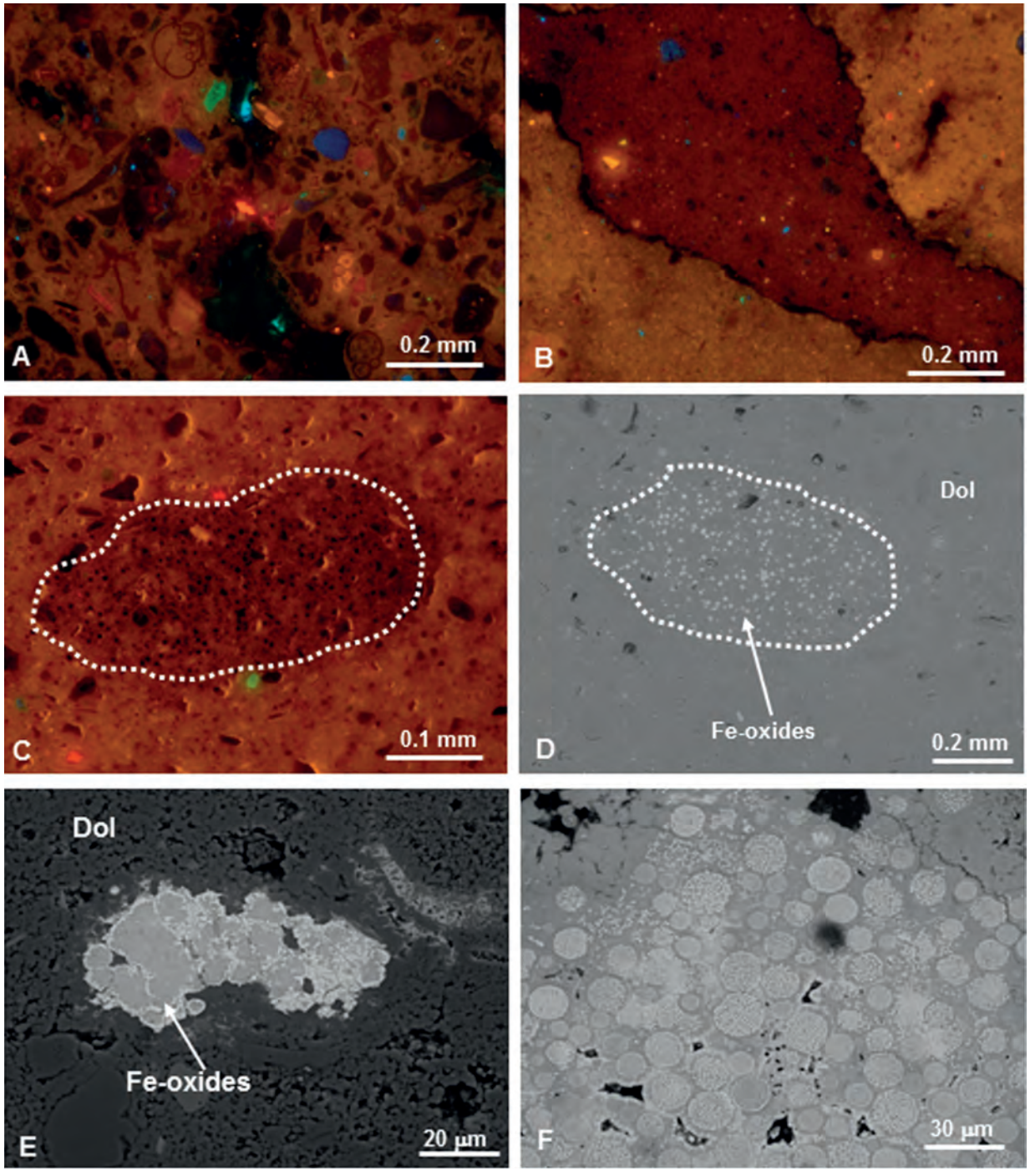

Isotopic composition ($\delta^{13}C$, $\delta^{18}O$, $^{87}Sr/^{86}Sr$)

Isotopic ($\delta^{13}C$ and $\delta^{18}O$) data from the Ibérico, Cornide and Arcos mounds vary considerably, not only within each sample but also between the samples from the same mud mound. $\delta^{13}C$ values of carbonate concretions from the Diasom Field range between -48.3 and -10.9 ‰ V-PDB, and $\delta^{18}O$ between +2.4 and +7.6 ‰ V-PDB (Table 2).

The $\delta^{13}C$ values from the Ibérico mound oscillate between -45.3 and -14.7 ‰ V-PDB for dolomite and Fe-bearing dolomite samples, and from -36.7 to -32.5 ‰ V-PDB for ankerite (samples 219 and 291; Table 2). $\delta^{18}O$ values vary from +3.1 to +7.0 ‰ V-PDB in dolomite and Fe-bearing dolomite, and from +3.1 to + 8.9 ‰ V-PDB for ankerite samples (Fig.5). All the samples analysed from the Cornide mound are dolomite and Fe-bearing dolomite, and their $\delta^{13}C$ and $\delta^{18}O$ values range from -48.3 to -14.4 ‰ V-PDB and from +5.7 to +7.6 ‰ V-PDB, respectively. HMC samples from the Arcos mound show the highest values in $\delta^{13}C$, ranging between -29.3 and -10.9 ‰ V-PDB, and the lowest values of $\delta^{18}O$, from +2.2 to +3.6 ‰ V-PDB.

The $^{87}Sr/^{86}Sr$ values of the dolomite samples from the Ibérico and Cornide mounds vary between 0.70933 and 0.70901 (Table 4) and a HMC carbonate concretion from the Arcos mound shows a value of 0.70881.

Discussion

The methane signature of the carbonate concretions

The $\delta^{13}C$ values provide insights into the origin of CO_2 involved in the formation of the carbonate concretions (Irwin *et al.,* 1977). The wide range of $\delta^{13}C$ values between -48.3 and -10.9 ‰ V-PDB (Fig. 6) observed in carbonate concretions from the Diasom Field strongly suggests a mixing of DIC from different sources during carbonate precipitation.

HMC samples and most dolomite concretions from the Arcos mound, and some dolomite concretions from the Cornide mound display $\delta^{13}C$ values ranging from -29.3 to -10.9 ‰ V-PDB (Fig. 6). These values are enriched in ^{13}C with respect to the rest of the samples analysed. The range of values records the precipitation of carbonates with large contributions of CO_2 derived from bacterial sulphate reduction (BSR) and/or remineralisation of organic matter (OM) ($\delta^{13}C_{OM}$ around -20 ‰ V-PDB, Irwin *et al*., 1977). The majority of dolomite and Fe-bearing dolomite concretions from the Ibérico and Cornide mud mounds show $\delta^{13}C$ values between -45 and -25 ‰ V-PDB. The highest $\delta^{13}C$ values may be attributed to CO_2 derived from bacterial sulphate reduction (e.g. Mazzini *et al*., 2004; Canet *et al*., 2006) and/or to organic matter oxidation (e.g., Mazzini *et al*., 2004). The depleted values maybe due to CO_2 inputs derived from sulphate-dependent AOM (Boetius *et al*., 2000; Michaelis *et al*., 2002).

Methane involved in the formation of concretions in the Diasom Field is probably thermogenic, as suggested by the $\delta^{13}C_{carbonate}$ values, which exceeded -40 ‰ V-PDB (e.g., Kaplan *et al*, 1997; Han *et al*., 2004). The contribution of thermogenic methane is corroborated by chemical data of the hydrocarbon gases and by the $\delta^{13}C$ of methane in mud volcanoes from the same area (Stadnitskaia *et al*., 2006; Nuzzo *et al*., 2009). Similar values have also been recorded in other authigenic carbonate concretions dredged from the Gulf of Cadiz (Díaz del Río *et al*., 2003; Magalhães, 2007;

Figure 4. Main cathodoluminescence (CL) and SEM features of carbonate concretions from the Ibérico, Cornide and Arcos mud mounds. A) Detail of a wackestone-packstone matrix displaying a medium-bright orange luminescence. The blue crystals correspond to detrital quartz and the green ones to feldspars. Planktonic foraminifera (*Pulleniatina sp*) are also observed in the upper part of the photo. CL image, Ibérico mound, sample 217; B) Detail of a filled burrow (unidentified ichnogenus). Luminescence of filling sediment, composed by a mixture of carbonate and Fe-oxides, is darker than the mudstone-wackestone matrix. CL image, Ibérico mound, sample 217; C) Sedimentary infilling of a bioturbation (*Chondrites* ichnogenus) (marked by the white pointed line). Dark points inside correspond to Fe-oxides. CL image, Cornide mound, sample 266; D) the same situation as the previous image C. White points inside are Fe-oxides (white pointed line). SEM (backscattered electrons -BS- image), Ibérico mound, sample 266; E) Fe-oxides filling porosity. SEM (BS image), Arcos mound, sample 233; and F) framboidal morphologies of Fe-oxides filling porosity. SEM (BS image), Arcos mound, sample 280.

Figura 4. *Principales características observadas mediante cátodo-luminiscencia (CL) y SEM de las concreciones carbonatadas de los montículos de fango Ibérico, Cornide y Arcos. A) Detalle de la matriz con textura 'wackestone-packstone'. La matriz muestra una luminiscencia media-brillante anaranjada. Los cristales azules corresponden a granos detríticos de cuarzo y los verdes a feldespatos. En la parte superior de la foto se observa un foraminífero planctónico (género Pulleniatina sp). Imagen de CL, montículo Ibérico, muestra 217; B) Bioturbación rellenada (icnogénero sin identificar) cuya luminiscencia es más oscura que la de la matriz ("mudstone-packstone"). El relleno está constituido por carbonato, componentes detríticos y óxidos de Fe (luminiscencia oscura). Imagen de CL, montículo Ibérico, muestra 217; C) Relleno de bioturbación (icnogénero Chondrites) limitado por una línea blanca punteada. Dentro de la misma hay puntos oscuros que corresponden a óxidos de Fe. Imagen de CL, montículo Cornide, muestra 266; D) Misma situación que la foto anterior. Los puntos blancos dentro de la bioturbación son óxidos de Fe (línea blanca punteada). SEM (imagen de electrones retrodispersados_BS), montículo Ibérico, muestra 266; E) Porosidad rellena de óxidos de Fe. SEM (imagen de BS), montículo Arcos, muestra 233; y F) Morfología framboidal de óxidos de Fe presentes en la porosidad. SEM (imagen de BS), montículo Arcos, muestra 280.*

Mud Mound	Sample	% Calcite	% mol Mg Calcite	% Dol/Ank	% mol Mg Dolomite	% mol Fe dolomite	% carbonate	% Quartz	$\delta^{13}C$ (‰ V-PDB)	$\delta^{18}O$ (‰ V-PDB)
Ibérico	214c.1	20	11	66	46	10	86	11	-38.0	+5.6
Ibérico	214c.2	32	11	60	43	16	92	8	-37.1	+5.2
Ibérico	215d.2	13	n.d.	38	44	13	51	49	-39.8	+3.7
Ibérico	215d.3	18	1	38	46	10	56	44	-37.5	+3.9
Ibérico	215d.4	19	3	40	46	10	59	40	-38.1	+4.9
Ibérico	215d.5	16	1	37	47	6	53	40	-36.6	+4.0
Ibérico	215d.6	18	1	44	44	13	63	32	-37.5	+3.8
Ibérico	216B.1	16	1	19	47	6	35	61	-31.5	+3.8
Ibérico	216B.2	19	3	26	47	6	45	48	-28.3	+3.3
Ibérico	216B.3	13	1	14	47	6	28	71	-29.4	+3.5
Ibérico	216B.4	24	1	32	47	6	56	39	-26.9	+3.1
Ibérico	216B.5	20	1	31	46	10	51	42	-33.2	+3.6
Ibérico	216B.6	35	11	26	47	6	61	36	-23.5	+3.3
Ibérico	217d.1	19	1	47	46	10	67	30	-14.7	+4.1
Ibérico	217d.2	40	3	38	47	6	78	21	-32.7	+4.0
Ibérico	217d.3	15	3	50	47	6	65	32	-34.4	+4.0
Ibérico	217d.4	21	3	46	46	10	67	32	-31.3	+4.0
Ibérico	218d.1	31	1	60	43	16	91	9	-35.0	+4.6
Ibérico	218d.2	24	n.d.	60	43	16	84	9	-38.4	+5.0
Ibérico	219C.1	21	n.d.	47	43	16	68	28	-34.0	+3.9
Ibérico	219C.2	30	1	32	34	35	62	38	-32.5	+8.9
Ibérico	219c.3	24	1	47	44	13	71	29	-35.1	+3.8
Ibérico	219c.4	30	1	39	38	26	69	31	-34.2	+3.1
Ibérico	265A.1	19	1	53	44	13	73	23	-36.8	+4.3
Ibérico	265A.2	32	1	30	44	13	62	38	-33.5	+3.8
Ibérico	265A.3	13	3	50	44	13	63	37	-38.4	+4.2
Ibérico	266A.1	6	n.d.	78	46	10	84	16	-43.0	+6.5
Ibérico	266A.2	n.d.	n.d.	85	46	10	85	15	-45.1	+7.0
Ibérico	266A.3	3	5	84	46	10	87	13	-45.3	+6.9
Ibérico	266A.4	16	8	70	44	13	85	15	-36.8	+5.7
Ibérico	266A.5	3	1	75	46	10	78	22	-44.7	+6.2
Ibérico	267B.1	27	1	34	44	13	61	35	-25.8	+3.8
Ibérico	267b.2	21	1	43	44	13	64	36	-29.3	+3.8
Ibérico	267b.3	15	1	27	44	13	42	55	-31.5	+4.1
Ibérico	267b.4	17	1	41	46	10	59	29	-33.9	+4.5
Ibérico	291c.1	39	3	52	40	22	91	9	-33.8	+4.3
Ibérico	291c.2	32	3	60	46	10	92	8	-33.7	+4.7
Ibérico	291c.3	6	3	92	41	19	98	2	-34.9	+5.6
Ibérico	291c.4	29	3	60	43	16	89	11	-36.7	+4.8
Ibérico	292.A.1	11	8	79	44	13	89	11	-36.5	+6.7
Ibérico	292.A.2	8	8	82	46	10	90	8	-40.6	+6.8
Ibérico	292.A.3	7	8	82	43	16	89	11	-41.4	+6.8
Cornide	201b.1	2	n.d.	83	46	10	85	15	-48.3	+6.3
Cornide	201b.2	4	3	85	46	10	88	12	-47.1	+6.4
Cornide	239b.1	n.d.	n.d.	88	46	10	88	12	-35.5	+7.2
Cornide	239b.2	n.d.	n.d.	87	44	13	87	13	-30.6	+7.2
Cornide	239b.3	n.d.	n.d.	87	46	10	87	13	-30.9	+7.2
Cornide	239b.4	3	1	83	44	13	86	14	-33.9	+6.8
Cornide	239b.5	7	n.d.	79	44	13	86	14	-32.3	+6.2
Cornide	241d.1	3	13	78	46	10	81	15	-30.6	+7.2
Cornide	241d.2	n.d.	8	98	46	10	98	2	-34.1	+7.1
Cornide	243d.1	5	1	78	46	10	83	17	-32.4	+6.7

Mud Mound	Sample	% Calcite	% mol Mg Calcite	% Dol/Ank	% mol Mg Dolomite	% mol Fe dolomite	% carbonate	% Quartz	$\delta^{13}C$ (‰ V-PDB)	$\delta^{18}O$ (‰ V-PDB)
Cornide	243d.2	9	1	71	46	10	80	20	-23.9	+6.3
Cornide	243d.3	2	n.d.	84	46	10	85	15	-33.8	+6.8
Cornide	243d.4	9	1	73	46	10	82	18	-24.9	+6.6
Cornide	244b.1	n.d.	n.d.	87	44	13	87	13	-37.0	+7.1
Cornide	244b.2	7	1	78	46	10	85	15	-30.9	+6.7
Cornide	244b.3	6	1	81	44	13	88	12	-29.6	+6.9
Cornide	249c.1	12	n.d.	75	44	13	86	14	-32.6	+6.4
Cornide	250a.1	n.d.	n.d.	91	46	10	91	9	-42.8	+6.3
Cornide	250a.2	5	n.d.	79	44	13	83	17	-34.3	+6.6
Cornide	250a.3	n.d.	n.d.	83	43	16	83	17	-36.6	+6.9
Cornide	250a.4	n.d.	n.d.	86	46	10	86	14	-44.8	+6.7
Cornide	250a.5	n.d.	n.d.	89	47	6	89	11	-39.6	+5.7
Cornide	251a.1	3	2	88	44	13	91	9	-45.6	+6.8
Cornide	251a.2	1	2	87	46	10	88	12	-47.3	+6.9
Cornide	251a.3	6	n.d.	83	44	13	89	11	-38.1	+6.8
Cornide	252a.1	18	1	69	46	10	87	13	-32.4	+6.0
Cornide	252a.2	7	n.d.	76	44	13	83	17	-33.2	+6.6
Cornide	252a.3	23	3	64	46	10	88	12	-28.4	+5.9
Cornide	253e.1	8	n.d.	85	46	10	93	7	-23.3	+6.8
Cornide	253e.2	16	n.d.	72	46	10	88	12	-14.4	+7.0
Cornide	254b.1	n.d.	n.d.	96	44	13	96	4	-31.9	+7.2
Cornide	254b.2	n.d.	n.d.	90	44	13	90	10	-36.3	+7.2
Cornide	254b.3	n.d.	n.d.	82	46	10	82	18	-29.8	+7.5
Cornide	255b.1	n.d.	n.d.	89	46	10	89	11	-32.9	+7.3
Cornide	255b.2	n.d.	n.d.	90	46	10	90	10	-31.5	+7.1
Cornide	255b.3	n.d.	n.d.	88	44	13	88	12	-32.5	+7.3
Cornide	255b.4	n.d.	n.d.	86	46	10	86	14	-32.4	+7.6
Cornide	256b.1	4	8	87	46	10	90	10	-27.7	+7.2
Cornide	256b.2	22	10	67	47	6	89	11	-24.1	+6.3
Cornide	257b.1	6	n.d.	80	46	10	86	14	-37.9	+6.1
Cornide	257b.2	12	1	78	47	6	91	9	-32.3	+6.3
Cornide	257b.3	10	1	78	47	6	88	12	-32.9	+6.7
Cornide	258a.1	7	1	84	47	6	91	9	-42.2	+6.0
Cornide	258a.2	14	1	79	44	13	93	7	-33.1	+5.8
Cornide	258a.3	6	1	85	44	13	91	9	-40.9	+6.1
Cornide	259a.1	n.d.	n.d.	85	46	10	85	15	-31.8	+7.5
Cornide	259a.2	n.d.	n.d.	87	46	10	87	13	-32.0	+7.5
Cornide	259a.3	n.d.	n.d.	85	46	10	85	14	-34.4	+7.5
Cornide	259a.4	n.d.	n.d.	86	46	10	86	14	-30.6	+7.5
Cornide	260a.1	15	1	75	44	13	90	10	-33.2	+6.3
Cornide	260a.2	16	1	75	46	10	91	9	-27.1	+6.0
Cornide	260a.3	25	1	61	44	13	86	14	-18.0	+6.0
Arcos	230c.1	29	11	25	47	6	54	43	-13.7	+4.7
Arcos	230c.2	23	11	33	49	3	56	41	-13.0	+4.6
Arcos	230c.3	29	10	33	46	10	62	38	-18.0	+4.4
Arcos	230c.4	22	6	35	46	10	57	43	-20.1	+5.4
Arcos	230c.5	25	10	31	47	6	56	43	-18.3	+5.2
Arcos	232a.1	13	11	13	41	19	27	72	-28.8	+5.6
Arcos	232a.2	45	11	46	44	13	91	9	-26.8	+4.6
Arcos	233c.1	17	n.d.	75	43	16	92	8	-39.4	+5.2
Arcos	233c.2	18	3	73	43	16	92	8	-40.3	+5.2
Arcos	233c.3	30	1	61	44	13	91	9	-39.0	+4.9

Mud Mound	Sample	% Calcite	% mol Mg Calcite	% Dol/Ank	% mol Mg Dolomite	% mol Fe dolomite	% carbonate	% Quartz	$\delta^{13}C$ (‰ V-PDB)	$\delta^{18}O$ (‰ V-PDB)
Arcos	234b.1	55	3	17	47	6	72	28	-17.9	+2.8
Arcos	234b.3	55	5	18	43	16	73	27	-15.8	+2.9
Arcos	238a.1	n.d.	n.d.	93	47	6	93	7	-37.3	+6.7
Arcos	238a.2	n.d.	n.d.	94	46	10	94	6	-37.2	+6.9
Arcos	238a.3	n.d.	n.d.	93	46	10	93	7	-37.1	+7.0
Arcos	278b.1	15	n.d.	57	43	16	72	28	-32.6	+5.0
Arcos	278b.2	15	1	52	44	13	67	33	-34.5	+4.6
Arcos	278b.3	35	1	34	43	16	69	28	-30.5	+3.8
Arcos	279.D.1	65	8	n.d.	44	13	65	35	-22.7	+2.7
Arcos	279.D.2	47	8	7	49	3	54	46	-26.7	+2.4
Arcos	279.D.3	49	8	6	49	3	55	45	-17.9	+2.6
Arcos	279.D.4	52	8	5	49	3	56	44	-12.1	+2.4
Arcos	279.D.5	52	8	4	49	3	55	45	-16.8	+2.8
Arcos	279.D.6	57	8	6	50	0	63	37	-10.9	+2.8
Arcos	280.A.1	61	5	n.d.	38	26	61	39	-18.9	+2.9
Arcos	280.A.2	58	11	n.d.	44	13	58	42	-29.3	+2.7
Arcos	280.A.3	58	5	5	46	10	62	38	-28.8	+2.4
Arcos	281.A.1	55	5	n.d.	46	10	55	45	-26.8	+2.5
Arcos	282.C.1	56	8	n.d.	47	6	56	44	-13.6	+2.2
Arcos	282.C.2	62	6	n.d.	n.d.	n.d.	62	38	-18.6	+2.6
Arcos	282.C.3	70	10	n.d.	n.d.	n.d.	70	30	-28.3	+2.9
Arcos	284.A.1	36	10	19	46	10	55	45	-16.7	+3.4
Arcos	284.A.2	33	11	20	44	13	53	47	-19.9	+3.6

Table 2. Summary of mineralogy (XRD) and isotopic composition data from Ibérico, Cornide and Arcos carbonate concretions. n.d.: not detected.
Tabla 2. *Resumen de la mineralogía (DRX) y de los datos de composición isotópica obtenidos en las concreciones carbonatadas de los montículos de fango Ibérico, Cornide y Arcos. n.d.: no detectado.*

Magalhães *et al.,* 2012; Vanneste *et al.,* 2012). However, an influence of microbial methane cannot be ruled out since $\delta^{13}C$ values below -40 ‰ V-PDB (within the isotopically undefined area of thermogenic and microbial origin; see Kaplan *et al*., 1997) have also been recorded (Fig. 6). Stadnitskaia *et al*. (2007) showed $\delta^{13}C$ values of methane ranging from -63 to -33 ‰ V-PDB in mud volcanoes of the Gulf of Cadiz. This suggests the presence of biogenic gas given that thermogenic methane (-50 to -30 ‰ V-PDB) is less ^{13}C-depleted than the microbial methane (-110 to -50 ‰ V-PDB) (Whiticar, 1999).

The origin of parental fluids

$\delta^{18}O_{fluidV\text{-}SMOW}$ (Vienna Standard Mean Ocean Water) of the parental fluid may be calculated by using two parameters: $\delta^{18}O_{carbonateV\text{-}PDB}$ and the fluid temperature during carbonate precipitation. It was not possible to obtain the fluid temperature directly due to the absence of fluid inclusions in the carbonate concretions. The present day seawater temperature in the Gulf of Cadiz at the depth of the mud volcanoes is 13-14°C (Gardner, 2001; Ambar *et al*., 2002; Díaz del Río *et al*., 2003; Hensen *et al*., 2007). A temperature of 14 °C was assumed to reflect the most probable pore water palaeotemperature and was used to calculate the $\delta^{18}O_{V\text{-}SMOW}$ of the parental fluid, using the following equations:

- High magnesium calcite (HMC; Friedman and O Neill, 1977): $\delta^{18}O_{fluidV\text{-}SMOW} = (\exp [\ln (1000 + \delta^{18}O_{HMC\text{-}VPDB}) - (18.030 / (273 + t)) + 0.03242]\text{-}1000) * 1.03086 + 30.86$
- Dolomite and Fe-bearing dolomite (Friedman and 0 Neil,1977): $\delta^{18}O_{fluidV\text{-}SMOW} - \delta^{18}O\ V_{dolomiteV\text{-}PDB} = (3.2x10^6/(273.15+t)^2) - 1.50$
- Ankerite (Fisher and Land, 1986): $\delta^{18}O_{fluidV\text{-}SMOW} - \delta^{18}O_{LMCV\text{-}PDB} = (2.78x10^6/(273.15+t)^2) + 0.11$
  where = temperature in Celsius degrees(°C)

Magalhães *et al.* (2012) used two temperatures (4 and 14 °C) to calculate the $\delta^{18}O_{fluidV\text{-}SMOW}$ but found no significant differences.

The whole set of $\delta^{18}O_{carbonate}$ values ranges from +2.4

Mund Mound	Sample	% CaO	% MgO	% SrO	% MnO	% FeO	% SiO2
Ibérico	215D.1	26.52	2.63	0.08	0.07	4.97	0.98
Ibérico	267B.2	22.38	7.22	0.06	0.05	2.81	0.87
Ibérico	291C.3	26.74	8.40	0.09	0.06	5.40	1.48
Cornide	252A.3	26.13	10.48	0.10	0.06	3.17	0.99
Cornide	253E.2	24.02	12.13	0.15	0.07	3.51	0.99
Cornide	260A.1	26.94	12.92	0.10	0.07	1.91	0.90
Arcos	234B.2	25.36	4.55	0.07	0.05	3.65	1.49
Arcos	233C.1	27.07	11.83	0.12	0.06	5.25	1.12
Arcos	282C.1	30.48	2.38	0.10	0.03	2.34	0.91

Table 3. ICP-MS chemical data of bulk samples from the Ibérico, Cornide and Arcos mud mounds (as wt % oxides).
Tabla 3. *Datos de composición química (ICP-MS) en muestras de roca total de los montículos de fango Ibérico, Cornide y Arcos (expresados como % en peso).*

to +7.6 ‰ V-PDB. Furthermore, most bulk samples are mixtures of dolomite, Fe-bearing dolomite, HMC and ankerite. For this reason, only samples bearing 70 to 100 wt % of any of these minerals was used to calculate the $\delta^{18}O_{fluid}$. Dolomite and Fe-bearing dolomites from the Ibérico mound (samples 266 and 292) have $\delta^{18}O_{carbonate}$ values ranging between +5.7 and +7.0 ‰ V-PDB (Tables 2 and 3). Therefore, their calculated $\delta^{18}O_{fluid}$ values oscillated between +3.0 and +3.7 ‰ (V-SMOW). The calculated $\delta^{18}O_{fluid}$ for parental fluids in equilibrium with ankerite (sample 219) varied between +1.2 and +2.9 ‰ V-SMOW.

The highest $\delta^{18}O_{carbonate}$ values (+6.6 to +7.6 ‰ V-PDB) are found in the dolomite and Fe-bearing dolomite (samples 239, 250, 254, 259; Table 2) from the Cornide mud mound. Assuming that these carbonate minerals precipitated at 14° C, the calculated $\delta^{18}O_{fluid}$ values are between +3.5 and +4.0 ‰ V-SMOW.

Theoretically, fluids involved in the precipitation of HMC (Arcos) and ankerite (Ibérico) concretions show $\delta^{18}O$ in the range of +0.9 to +2.9 ‰ V-SMOW. The lowest values may be due to precipitation in equilibrium with seawater ($\delta^{18}O$ bottom seawater in the Gulf of Cadiz: +0.5 and +1.5 ‰ V-SMOW, Mazurenko *et al.*, 2002). Values exceeding +1.5 ‰ V-SMOW suggest precipitation from seawater modified pore fluids caused by rock-water interaction. Another explanation for the relatively high calculated $\delta^{18}O_{fluid}$ could be the contribution of ^{18}O-enriched fluids generated by gas-hydrate decomposition (e.g., Greinert *et al.*, 2001; Mazzini *et al.*, 2006; Naehr *et al.*, 2007). An ^{18}O enrichment of +3.0 ± 0.1 ‰ V-SMOW (Davidson and Least, 1983; Suess *et al.*, 1999) occurs in the hydrate water with respect to pore water during gas-hydrate formation (Mazurenko *et al.*, 2002 and 2003).

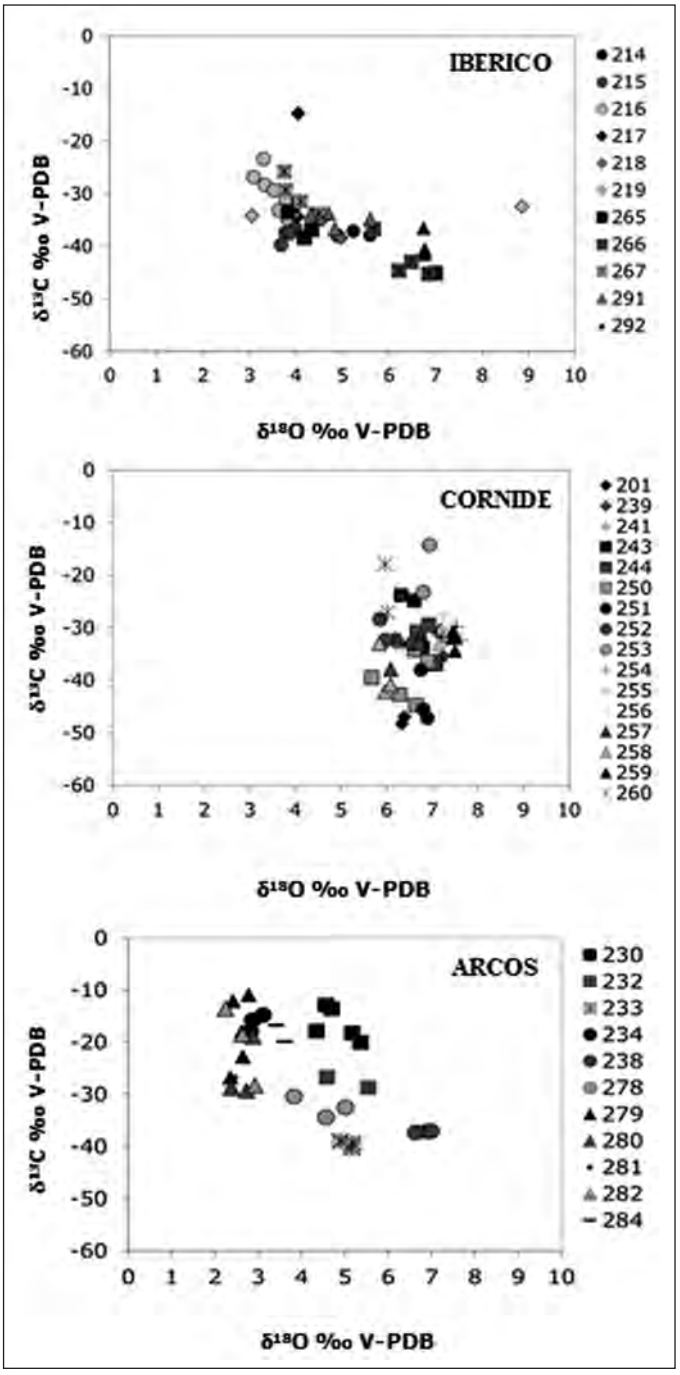

Figure 5. Isotopic compositions of carbonate concretions from the Ibérico, Cornide and Arcos mud mounds.
Figura 5. *Composiciones isotópicas de las concreciones carbonatadas de los montículos de fango Ibérico, Cornide y Arcos.*

$\delta^{18}O_{fluid}$ values calculated from dolomite and Fe-bearing dolomite samples (Ibérico, Cornide and Arcos mud mounds) fluctuate between +3.0 and +3.9 ‰ V-SMOW, suggesting a gas-hydrate decomposition origin for the waters in which concretions precipita-

Mud mound	Sample	Mineralogy	$^{87}Sr/^{86}Sr$	$\delta^{13}C$ (V-PDB)	$\delta^{18}O$ (V-PDB)
IBÉRICO	291.C3	Dolomite	0.70933	-34.9	+5.6
CORNIDE	239.B1	Dolomite	0.70901	-35.5	+7.2
ARCOS	282.C3	HMC	0.70881	-28.3	+2.9

Table 4. $^{87}Sr/^{86}Sr$ results of bulk samples from the Ibérico, Cornide and Arcos mud mounds. Isotopic compositions ($\delta^{13}C$, $\delta^{18}O$) of the same samples have been added.
Tabla 4. *Resultados de $^{87}Sr/^{86}Sr$ de roca total en las muestras de los montículos de fango Ibérico, Cornide y Arcos. Se han añadido las composiciones isotópicas ($\delta^{13}C$, $\delta^{18}O$) de cada muestra.*

ted. Recent studies have shown similarly enriched $\delta^{18}O$ values (more than +2 ‰ V-SMOW) in other authigenic carbonates from the Gulf of Cadiz whose origin has also been attributed to fluids generated by gas hydrate decomposition (Magalhães *et al*., 2012; Vanneste *et al*., 2012). Nevertheless, the highest values of $\delta^{18}O$ cannot only be explained by the influence of gas-hydrate destabilisation; an input of ^{18}O-rich water of another provenance is necessary. Clay-mineral dehydration (probably deep-seated transformation smectite-illite) may be the main source of ^{18}O-enriched fluids (Dähmann and de Lange, 2003; Gontharet *et al*., 2007; Hensen *et al.,* 2007). Hensen *et al*. (2007) have obtained $\delta^{18}O$ values that reach + 8 ‰ V-SMOW.

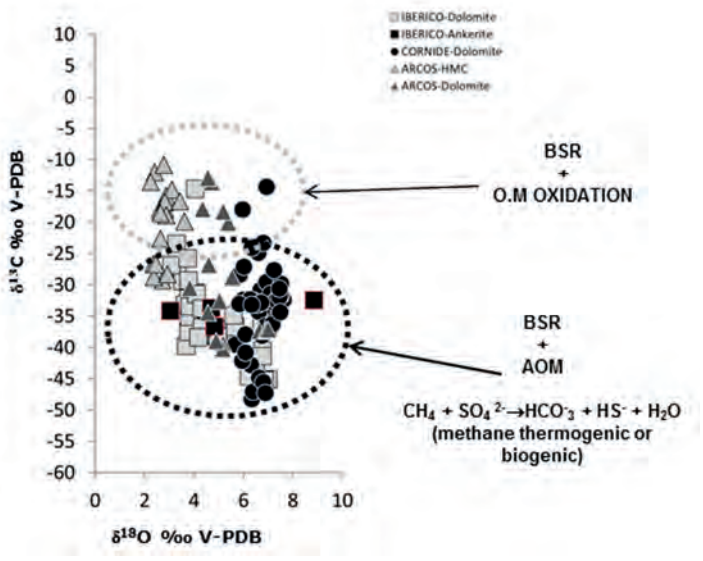

Figure 6. Isotopic compositions of all analysed samples. Values are plotted considering their mineralogy (dolomite, HMC or ankerite) and sampling site (Ibérico, Cornide and Arcos). The influence of the main biochemical processes that took place during the carbonate formation is marked with dotted lines.
Figura 6. *Composiciones isotópicas ($\delta^{13}C$, $\delta^{18}O$) de las muestras estudiadas. Los valores se han representado teniendo en cuenta la mineralogía de las muestras (dolomita, HMC o ankerita) y el lugar de procedencia (Ibérico, Cornide o Arcos). El límite de influencia de los diferentes procesos bioquímicos que tuvieron lugar en la formación de estos carbonatos está marcado con líneas de puntos.*

The origin of the carbonate concretions in the Ibérico, Cornide and Arcos mud mounds

The mineralogical, petrological and geochemical data strongly suggest that carbonate concretions occurred in the sulphate reduction zone (SRZ), which is located below the oxic zone and above the methanogenic zone, and which can attain a thickness of several tens of metres (Irwin *et al*., 1977). Sulphate would be rapidly consumed in the SRZ, where methane flow circulation is linked to fractures or bioturbation, which increased the permeability into the sediment and the redistribution of fluids and organic matter. The marine Mg^{2+} concentration is preserved in the SRZ as it is not consumed as $MgSO_4$ (Baker and Kastner, 1981; Magalhães *et al*., 2012), which favours the precipitation of Mg-carbonates (HMC or dolomite) and inhibits the formation of low magnesium calcite (LMC) and aragonite (Folk, 1974). In addition to the high sulphate concentration (Chafetz *et al*., 1991; Burton, 1993; Savard *et al*., 1996; Kralj *et al*., 2004; Vanneste *et al*., 2012), other controlling factors of the $MgCO_3$ incorporation into calcite lattice are P_{CO2}, temperature and amount of phosphate (Burton, 1993). Sulphate and alkalinity decrease because of the presence of a high methane flux. This inhibits the precipitation of LMC and aragonite and leads to the formation of HMC (Greinert *et al*., 2001).

The biogeochemical processes that operate in the SRZ include remineralisation of organic matter (organo-sulphate reduction), or sulphate reduction coupled to the anaerobic methane oxidation (AOM). Based on $\delta^{13}C$ values, the remineralisation of organic matter probably played a central part in the formation of: 1) HMC from the Arcos mud mound, 2) the ankerite from the Ibérico, and 3) some dolomites from the Cornide and Arcos mounds. The role of BSR in these samples was also confirmed by the presence of Fe-oxides pseudomorphic after framboidal pyrite, indicating a bacterial origin (e.g., Hovland *et al*., 1987; Ritger *et al*., 1987; Wilkin and Barnes, 1997; Peckmann *et al*., 2001; Shapiro and Fricke, 2002; Chen *et al*., 2007; Gontharet *et al*. 2007). Framboidal morphologies indicate that BSR was active during carbonate formation because of the presence of sedimentary pyrite due to the combination of HS^- with dissolved iron (Berner, 1970; Vanneste *et al*., 2012). In contrast, in dolomite concretions from the Ibérico mound and in a few concretions from the Cornide mound, the $\delta^{13}C$

values suggest the presence of ^{13}C-depleted CO_2 due to AOM and, to a lesser extent, to methanogic derived CO_2 (Greinert *et al.*, 2001).

This variability of carbon sources (dissolved inorganic carbon, DIC) in the SRZ is also observed in the $^{87}Sr/^{86}Sr$ composition of the parental fluids. The presence of marine fluids and/or modified marine fluids is confirmed by the $^{87}Sr/^{86}Sr$ values (Table 4), which are close to the values of recent sea-water (0.709175; Paytan *et al.*, 1993). The marine signature is mainly detected in HMC and ankerite concretions, where lower $\delta^{18}O_{fluidV\text{-}SMOW}$ values were calculated. The strontium content in these samples is lower than in dolomite samples, indicating that precipitation took place under the influence of marine fluids (e.g., Savard *et al.*, 1996; Peckmann *et al.*, 2001; Mazzini *et al.*, 2006). The other source of fluids that may be present in the SRZ in the Diasom Field is attributed to the gas-hydrate destabilisation ($\delta^{18}O_{fluidV\text{-}SMOW}$ values higher than +1.5 ‰). This source appears to play a major role in the precipitation of dolomite and Fe-bearing dolomite concretions.

Conclusions

Carbonate concretions from the Diasom Field were commonly formed around bioturbation structures (burrows) and vary considerably in morphology and size. Dolomite, Fe-bearing dolomite, HMC and ankerite are the main carbonate minerals. Minor amounts of quartz and Fe-oxides are also found as accessory minerals. The only porosity found is due to bioturbation (burrows), bioerosion (borings) and intraparticle porosity in planktonic foraminifera.

The $\delta^{13}C$ values are extremely low between -48.3 and -10.9 ‰ V-PDB and their range suggests that the CO_2 involved in the carbonate precipitation had multiple sources. The main biogeochemical processes associated with these different sources of CO_2 are bacterial sulphate reduction (BSR), organic matter oxidation, anaerobic methane oxidation coupled to sulphate reduction (AOM) and methanogenesis.

The influence of AOM and CO_2 derived from methanogenes was mainly detected in samples from the Ibérico and Cornide mounds, whereas samples from the Arcos mud mound mainly suggest BSR and organic matter oxidation. The $\delta^{13}C_{carbonate}$ values indicate that the origin of methane is mainly thermogenic. The presence of microbial methane was only detected in some carbonate concretions from the Ibérico mound.

The main fluids involved in the precipitation of the carbonate concretions are probably related to gas hydrate destabilisation ($\delta^{18}O$ higher than +1.5 ‰V-SMOW) with a minor influence of seawater, and marine fluids enriched in ^{18}O due to rock-water interaction. Another provenance of these ^{18}O-rich fluids may be burial-diagenetic clay dehydration (transformation smectite-illite). In such a case, fluids can reach values of up to + 8 ‰ V-SMOW.

Morphological, mineralogical and geochemical variability recorded in the concretions of one mud mound may in part be due to the sampling system used: a rectangular benthic-type dredge with variable distances covered by each dredge (between 300 and 500 m). This suggests that concretions sampled together might correspond to variable environmental conditions (e.g., different methane flux derived from gas-hydrate destabilisation or local changes in the amount of available organic matter).

The concretions probably formed in the sulphate reduction zone (SRZ), which is characterised by the presence of dissolved SO_4^{2-}, the availability of organic matter and the circulation of methane. The widespread distribution of bioturbation increased the permeability of the sediment, favouring the redistribution of organic matter and the circulation of methane and fluids derived from gas-hydrate destabilisation.

Acknowledgements

This paper is dedicated to the memory of Jordi María de Gibert Atienza, our friend and colleague. The project was financed by the support of the ESF 01-LEC-EMA06F and the Spanish MEC Project REN 2002-11418-E projects. We are indebted to the technical team of the Institute of Earth Sciences Jaume Almera (ICTJA-CSIC) for the X-ray diffraction determinations (Josep Elvira); to the Serveis Cientifico-Tècnics of the University of Barcelona (CCiTUB) for the C, O isotopic analyses, the ICP-MS major element quantification and the electron microscope observations; to the LIFS unit in the department of Geochemistry, Petrology and Geological Prospection the University of Barcelona for the optical microscopy and cathodoluminescence facilities; and to the Geochron Laboratory from the Basque Country University for the $^{87}Sr/^{86}Sr$ isotopic ratio determinations. Finally, special thanks are due to the reviewers who have significantly improved the manuscript.

References

Aharon, P. 1994. Geology and biology of modern and ancient submarine hydrocarbon seep and vents: an introduction. *Geo-Marine Letters*, 14, 69-73.

Aloisi, G., Pierre, C., Rouchy, J.M., Foucher, J.P., Woodside, J. and the MEDINAUT Scientific Party 2000. Methane-related authigenic carbonates of eastern Mediterranean Sea mud volcanoes and their possible relation to gas hydrate destabilisation. *Earth and Planetary Science Letters,* 184, 321-338.

Ambar, I., Serra, N., Brogueria, M. J., Cabecadas, G., Abrantes, F., Freitas, P., Goncalves, G. and González, N. 2002. Physical, chemical and sedimentological aspects of the Mediterranean outflow off Iberia. *Deep Sea Research Part II: Topical Studies in Oceanograph,* 49 (19), 4163-4177.

Baker, P.A. and Kastner, M. 1981. Constrains on the formation of sedimentary dolomite. *Science,* 213 (4504), 214-216.

Banda, E., Torné, M. and Iberian Atlantic Margins Group 1995. Iberian Atlantic Margins Group investigates deep structure of ocean margins*, Eos Trans. AGU*,76 (3), 25, 28-29.

Berástegui, X., Banks, C., Puig, C., Taberner, C., Waltham, D. and Fernández, M. 1998. Lateral diapiric emplacement of Triassic evaporites at the southern margin of the Guadalquivir Basin, Spain. In: Mascle, A., Puigdefàbregas, C., Luterbacher, H.P. and Fernández, M. (eds.), *Cenozoic Foreland Basins of westerrn Europe*. Geological Society Special Publications, London, 49-68.

Berner, R.A. 1970. Sedimentary pyrite formation*. American Journal of Science*, 268 (1), 1-23.

Boetius, A., Ravenschlag, K., Schubert, C.J., Rickert, D., Widdel, F., Gieseke, A., Amann, R., Jorgense, B.B., Witte, U. and Pfannkuche, O. 2000. A marine microbial consortium apparently mediating anaerobic oxidation of methane. *Nature*, 407, 623-626.

Brown, K. and Westbrook, G.K. 1988. Mud diapirs and subcretion in the Barbados ridge accretionary complex: the role of fluids in accretionary processes. *Tectonics*, 7, 613-640.

Burhan, R. Y. P., Trendel, J. M., Adam, P., Wehrung, P., Albrecht, P. and Nissenbaum, A. 2002. Fossil bacterial ecosystem at methane seeps: origin of organic matter from Be'eri sulphur deposit, Israel. *Geochimica et Cosmochimica Acta*, 66, 4085-4101.

Burton, E. A. 1993. Controls on marine carbonate cement mineralogy: review and reassessment. *Chemical Geology*, 105, 163-179.

Burton,. E. A. and Walter, R L. M. 1987. Relative precipitation rates of aragonite and Mg calcite from seawater: Temperature or carbonate ion control?. *Geology*, 15, 111- 114.

Campbell, K.A. and Bottjer, D.J. 1993. Fossil cold seeps. *National Geographic Research & Exploration*, 9, 326-343.

Campbell, K.A., Farmer, J.D. and Des Marais, D. 2002. Ancient hydrocarbon seeps from the Mesozoic convergent margin of California: carbonate geochemistry, fluids and paleoenvironments. *Geofluids*, 2, 63-94.

Campbell, K.A. 2006. Hydrocarbon seep and hydrothermal vent paleoenvironments and palaeontology: Past developments and future research directions. *Palaeogeography, Palaeoclimatology, Palaeoecology*, 232, 362-407.

Canet, C., Prol-Ledesma, R.M., Escobar-Briones, E., Mortera-Gutiérrez, C., Lozano-Santa Cruz, R., Linares, C., Cienfuegos, E. and Morales-Puente, P. 2006. Mineralogical and geochemical characterization of hydrocarbon seep sediments from the Gulf of Mexico. *Marine and Petroleum Geology*, 23 (5), 605-619.

Cavagna, S., Clari, P. and Martire, L. 1999. The role of bacteria in the formation of cold seep carbonates: geological evidence from Monteferrato (Tertiary, NW Italy). *Sedimentary Geology*, 126, 253-270.

Chafetz, H.S., Rush, P.F. and Utech, N.M. 1991. Microenvironmental controls on mineralogy and habit of $CaCO_3$ precipitates: An example from an active travertine system. *Sedimentology*, 38, 107-126.

Chao, H.C. You, C.F: Liu, H.C. and Chung, C.H. 2013. The origin and migration of mud volcano fluids in Taiwan: Evidence from hydrogen, oxygen, and strontium isotopic compositions. *Geochimica et Cosmochimica Acta,* 114, 29-51.

Chen, Y., Matsumoto, R., Paull, C.K., Ussler III, W., Lorenson, T., Hart, P. and Winters, W. 2007. Methane-derived authigenic carbonates from the northern Gulf of México-MD02 Cruise. *Journal of Geochemical Exploration*, 95, 1-15.

Chung, F. H. 1974. Quantitative Interpretation of X-Ray Diffraction Patterns of Mixtures. I. Matrix-Flushing Method for Quantitative Multicomponent Analysis. *Journal of Applied Crystallography*, 7.519-525.

Clari, P., Fornara, L., Ricci, B. and Zuppi, G.M. 1994. Methane derived carbonates and chemosymbiotic communities of Piedmont (Miocene, northern Italy): an update. *Geo-Marine Letters*, 14, 201-209.

Claypool, G. E., and Kaplan, I. R., 1974. The origin and distribution of methane in marine sediments,. In: Kaplan, I.R. (ed.), *Natural Gasses in Marine Sediments*. Plenum Press, New York, 99-139

Conti, S., Fontana, D., Gubertini, A., Sighinolfi, G., Tateo, F., Fioroni, C. and Fregni, P. 2004. A multidisciplinary study ofMiddle Miocene seep-carbonates from the northern Apennine foredeep (Italy). *Sedimentary Geology*, 169, 1-19.

Dählmann, A. and de Lange, G.J. 2003. Fluid-sediment interactions at Eastern Mediterranean mud volcanoes: a stable isotope study from ODP Leg 160. *Earth and Planetary Science Letters,* 212, 377-391.

Davidson, D.W. and Leaist, D.G. 1983. Oxygen-18 enrichment in the water of a clathrate hydrate.*Geochimica et Cosmochimica Acta*, 47, 2293-2295.

de Boever, E., Swennen, R. and Dimitrov, L. 2006. Lower Eocene carbonate-cements "chimneys" structures (Varna, Bulgaria)- Control of seepage rates on their formation and stable isotopic signature. *Journal of Geochemical Exploration*, 89, 1-3, 78-82.

de Haas, H., Mienis, F. and Shipboard Scientific Crew.2005. Cold water corals and carbonate mound formation at the Pen Duick Escarpment (Gulf of Cadiz) and Rockall Bank. *Cruise report R. V. Pelagia cruise M2005 (64PE237)*. Royal Netherlands Institute for Sea Research, Texel.

Díaz del Río, V., Somoza L., Martínez-Frías J., Hernández-Molina, F.J., Lunar, R., Fernández-Puga, M.C., Maestro,

A., Terrinha, P., Llave, E., García A., García, A. C. and Vázquez, J.T. 2001. Carbonate chimneys in the Gulf of Cadiz: Initial report of their petrography and geochemistry. In: Akhmanov, G. and Suzyumov, A. (eds.), *Geological processes on deep-water European margins*. IOC-UNESCO Workshop Report, 175, 53-54.

Díaz-del-Río, V., Somoza, L., Martínez-Frías. J., Mata, M.P., Delgado. A., Hernández-Molina, F.J., Lunar. R., Martín-Rubí. J.A., Maestro. A., Fernández-Puga. M.C., León. R., Llave. E., Medialdea. T. and Vázquez, J.T. 2003. Vast fields of hydrocarbon-derived carbonate chimneys related to the accretionary wedge/olistostrome of the Gulf of Cadiz. *Marine Geology*, 195, 177-200.

Fernández-Puga, M.C., Vázquez, J.T., Somoza, L., Díaz del Río, V., Medialdea, T., Mata, M.P., and León, P. 2007. Gas-related morphologies and diapirism in the Gulf of Cadiz. *Geo-Marine Letters*, 27, 213-221.

Fisher, R. E. and Land, L. S. 1986. Diagenetic history of Eocene Wilcox sandstones, South-Central Texas. *Geochimica et Cosmochimica Acta*, 50 (4), 551-561.

Flinch, J.F. 1996. Accretion and extensional collapse of the external western Rif (Northern Morocco). In: Ziegler, P.A., Horvath, F. (eds.), *Peri-Tethys Memoir 2: Structure and Prospects of Alpine Basins and Forelends*. Mémories du Museum National d Historie naturelle, Paris, 61-85.

Folk, R. L. 1974. The Natural history of crystalline calcium carbonate: Effect of magnesium content and salinity. *Journal of Sedimentary Petrology*, 44.40-53.

Formolo, M.J., Lyons, T.W., Zhang, C.L., Kelley, C., Sassen, R., Horita, J. and Cole, D.R. 2004. Quantifying carbon sources in the formation of authigenic carbonates at gas hydrate sites in the Gulf of Mexico. *Chemical Geology*, 205, 253-264.

Friedman, I. and O Neil, J.R. 1977. Compilation of stable isotope fractionation factors of geochemical interest. In: M-Fleicher, M. (ed.), *Data of geochemistry*. Geological Survey Professional Paper, 440, KK1-KK12.

Gardner, J. 2001. Mud volcanoes revealed and sampled on the Western Moroccan continental Margin. *Geophysical Research Letters*, 28, 339-342.

Gill, F.L., Harding, I.C., Little, C.T.S, and Todd, J.A. 2005. Palaeogene and Neogene cold seep communities in Barbados, Trinidad and Venezuela: an overview. *Palaeogeography, Palaeoclimatology, Palaeoecology*, 227, 191-209.

Gontharet, S., Pierre, C., Blanc Valleron, M., Rouchy, J.M., Fouquet, Y., Bayon G., Foucher, J.P., Woodside, J., Mascle, J. and the Nautinil Scientific Party. 2007. Nature and origin of diagenetic carbonate crusts and concretions from mud volcanoes and pockmarks of the Nile deep sea fan (eastern Mediterranean Sea). *Deep Sea Research II*, 54, 1292-1311.

Goldsmith, J. R., Graf, D. L. and Heard, H. C. 1961. Lattice constants of the calcium-magnesium carbonates. *American Mineralogist*, 46, 453-457.

González, A., Córdoba, D., Vegas R. andMatías, L.M. 1998. Seismic crustal structure in the south west of the Iberian Peninsula and the Gulf of Cadiz. *Tectonophysics*, 296, 317-331.

Gràcia, E., Dañobeitia, J., Vergés, J. and Bartolomé, R. 2003. Crustal architecture and tectonic evolution of the Gulf of Cadiz (SW Iberian margin) at the convergence of the Eurasian and African plates. *Tectonics*, 22 (4), 1033-1051.

Greinert, J., Bohrmann, G. and Suess, E. 2001. Gas hydrate-associated carbonates and methane-venting at Hydrate Ridge: classification, distribution and origin of authigenic lithologies. In: Paull, C.K., and Dillon, W.P. (eds.), *Natural Gas Hydrates: Occurrence, Distribution, and Detection.* American Geophysical Union, Geophysical Monograph Series, 124, 99-114.

Greinert, J., Bollwerk, S.M., Derkachev, A., Bohrmann, G. and Suess, E. 2002. Massive barite deposits and carbonate mineralization in the Derugin Basin, Sea of Okhotsk: precipitation processes at cold seep sites. *Earth and Planetary Science Letters*, 203, 165-180.

Haffert, L., Haeckel, M., Lebetraua, V., Berndt, C., Hensen, C., Nuzzo, M., Reitz, A., Scholz, F., Schönfeld, J., Pérez-García, C. and Weise, S.M. 2012. Fluid evolution and authigenic mineral paragenesis related to salt diapirism - The Mercator mud volcano in the Gulf of Cadiz. *Geochimica et Cosmochimica Acta*,106, 261-286.

Han, X., Suess, E., Sahling, H. and Wallmann, K. 2004. Fluid venting activity on the Costa Rica margin: new results from authigenic carbonates. *International Journal of Earth Science*s, 93 (4), 596-611.

Hensen, Ch., Nuzzo, M., Hornibrook, E., Pinheiro, L.M., Bock, B., Magalhães, V.H. and Bruckmann, W. 2007. Sources of mud volcano fluids in the Gulf of Cadiz- indications for hydrothermal imprint.*Geochimica et Cosmochimica Acta*, 71, 1232-1248.

Hernández-Molina, F.J., Llave, E., Somoza, L., Fernández-Puga, M.C., Maestro, A., León, R., Medialdea, T., Barnolas, A., García, M., Díaz del Río, V., Fernández-Salas, L.M., Vázquez, J.T., Lobo, F.J., Alveirinho-Dias, J.A., Rodero, J., Gardner, J. 2003. Looking for clues to paleoceanographic imprints: A diagnosis of the Gulf of Cadiz contourite depositional systems. Geology, 31, 19-22.

Hovland, M., Talbot, M.R., Qvale, H., Olaussen, S. and Aasberg, L. 1987. Methane-related carbonate cements in pockmarks of the North Sea. *Journal of Sedimentary Petrology*, 57 (5), 881-892.

Iribarren, L., Vergés, J., Camurri, F., Fullea, J. and Fernández, M. 2007. The structure of the Atlantic-Mediterranean transition zone from the Alboran Sea to the Horseshoe Abyssal Plan (Iberia-Africa plate boundary). *Marine Geology*, 243, 97-119.

Irwin, H., Curtis, Ch. and Coleman, M.1977. Isotopic evidence for source of diagenetic carbonates forms during burial of organic-rich sediments. *Nature*, 269, 209-213.

Kaplan, I.R., Galperin, Y., Lu, S.T. and Lee, R.P. 1997. Forensic Environmental Geochemistry: differentiation of fuel types, their sources and release times. *Organic Geochemistry*, 27, 289-317.

Kauffman, E. G., Arthur, M. A., Howe, B. and Scholle, P. A. 1996.Widespread venting of methane-rich fluids in Late Cretaceous (Campanian) submarine springs (Tepee Buttes), Western Interior seaway, U.S.A. *Geology*, 24,9, 799-802.

Kelly, J.R.A., Ditchfield, P.W., Doubleday, P.A. and Marshall, J.D. 1995. An Upper Jurassic methane-seep limestone from the Fossil Bluff Group forearc basin of Alexander island, Antarctica. *Journal of Sedimentary Research*, 65, 274-282.

Kralj, D., Kontrec, J., Brecevic, L., Falini, G. and Nothig-Laslo, V. 2004. Effect of inorganic anions on the morphology and structure of magnesium calcite. *Chemistry-A European Journal*, 10 (7), 1647-1656.

Kulm, L. D., Suess, E., Moore, J.C., Carson, B., Lewis, B.T., Ritger, S., Kadko, D., Thornburg, T., Embley, R., Rugh, W., Massoth, G.J., Langseth, M., Cochrane, G.R. and Scamman, R.L. 1986. Oregon subduction zone: Venting, fauna and carbonates. *Science*, 231, 561-566.

Lobo, F. J., Hernández-Molina, F.J., Somoza, L., Rodero, J., Maldonado, A. and Barnolas, A. 2000. Patterns of bottom current flow deduced from dune asymmetries over the Gulf of Cadiz shelf (southwest Spain). *Marine Geology*, 164, 91-117.

Magalhães, V.H. 2007. Authigenic carbonates and fluid escape structures in the Gulf of Cadiz. Doctoral Thesis, University of Aveiro, Aveiro, 421 pp.

Magalhães, H, V., Pinheiro, L., Ivanov, M. K., Kozlova, E., Blinova, E., Kolganova, J., Vasconcelos, C., McKenzie, J. A., Bernasconi, S. M., Kopf, A. J, Díaz-del-Río, V., González, F. J. and Somoza, L. 2012. Formation processes of methane-derived authigenic carbonates from the Gulf of Cadiz. *Sedimentary Geology*, 243-244, 155-168.

Maldonado, A., Somoza, I. and Pallarés, L. 1999. The Betic orogen and the Iberian-African boundary in the Gulf of Cadiz: geological evolution (central North Atlantic). *Marine Geology*, 155, 9-43.

Mata, P., Williams, L.B, Nieto, F., Martos, R. and Sainz-Díaz, C.I. 2012. Preliminary B and Li Isotope Data of Illite/Smectite from Mud Volcano Sediments from the Gulf of Cadiz. *Macla*, 16, 100-101

Mazurenko, L.L., Soloviev, V.A., Belenkaya, I., Ivanov, M.K. and Pinheiro, L.M. 2002. Mud volcano gas hydrates in the Gulf of Cadiz. *Terra Nova*, 14, 321-329.

Mazurenko, L.L., Soloviev, V.A., Gardner, J.M. and Ivanov, M.K. 2003. Gas hydrates in the Ginsburg and Yuma mud volcano sediments (Moroccan Margin): results of chemical and isotopic studies of pore water. *Marine Geology,* 195, 201-210.

Mazzini, A., Ivanov, M.K., Parnell, J., Stadnitskaia, A., Cronin, B.T., Poludetkina, E., Mazurenko, L. and van Weering, T.C.E. 2004. Methane-related authigenic carbonates from the Black Sea: geochemical characterisation and relation to seeping fluids. *Marine Geology*, 212, 153-181.

Mazzini, A., Svensen, H., Hovland, M. and Planke. S. 2006. Comparison and implications from strikingly different authigenic carbonates in a Nyegga complex pockmark, G11, Norwegian Sea. *Marine Geology*, 231, 89-102.

Medialdea, T., Vegas, R., Somoza, L., Vázquez, J.T., Maldonado, A., Díaz del Río, V., Maestro, A., Córdoba, D. and Fernández-Puga, M.C. 2004. Structure and evolution of the "Olistrostome" complex of the Gibraltar arc in the Gulf of Cadiz (eastern Central Atlantic): evidence from two long seismic cross-sections. *Marine Geology*, 209, 173-198.

Michaelis, W., Seifert, R., Nauhaus, K.,Treude, T., Thiel, V., Blumenberg, M., Knittel, K., Gieseke, A., Peterknecht, K., Pape, T., Boetius, A., Amann, R., Jorgensen, B.B., Widdel, F., Peckmann, J., Pimenov, N.V. and Gulin, M. 2002. Microbial reefs in the Black Sea fuelled by anaerobic oxidation of methane. *Science*, 297, 1013-1015.

Mienis, F., de Haas, H. and Shipboard Scientific Party 2004. Report of cruise "Moundforce 2004" with Royal R.V. Pelagia. *The distribution, morphology, sedimentology and watermass characteristics of and around mounds in the Gulf of Cadiz and the SW Rockall Trough Margin*. Unpublished cruise report Royal Netherlands Institute for Sea RESEACH, 100 pp.

Naehr, T.H., Eichhubl, P., Orphan, V.J., Hovland, M., Paull, C.K., Ussler III, W., Lorenson, T.D. and Greene, H.G. 2007. Authigenic carbonate formation at hydrocarbon seeps in continental margin sediments. A comparative study. *Deep-sea Research* II, 54, 1268-1291.

Nuzzo, M., Hornibrook, E. R. C., Gill, F., Hensen, C., Pancost, R. D., Haeckel, M., Reitz, A., Scholz, F., Magalhães, V. H., Brueckmann, W. and Pinheiro, L. M. 2009. Origin of light volatile hydrocarbon gases in mud volcano fluids, Gulf of Cadiz - Evidence for multiple sources and transport mechanisms in active sedimentary wedges. *Chemical Geology*, 266, 359-372.

Paytan, A., Kastnet, M., Martín, E.E., Macdougall, J.D. and Herbert, T. 1993. Marine barite as a monitor of seawater strontium isotope composition. *Nature*, 366, 445-449.

Peckmann, J., Walliser, O.H., Riegel, W. and Reitner, J. 1999. Signatures of hydrocarbon venting in a Middle Devonian carbonate mound (Hollard Mound) at the Hamar Laghdad (Antiatlas, Morocco).*Facies,* 40, 281-296.

Peckmann, J., Reimer, A., Luth, U., Luth, C., Hansen, B.T., Heinicke, C., Hoefs, J. and Reitner, J. 2001. Methane-derived carbonates and authigenic pyrite from the north-western Black Sea. *Marine Geology*, 177, 129-150.

Peckmann, J., Goedert, J.L., Thiel, V., Michaelis, W. and Reitner, J. 2002. A comprehensive approach to the study of methane-seep deposits from the Lincoln Creek Formation, western Washington State, USA. *Sedimentology*, 49, 855-873.

Peckmann, J. and Thiel, V. 2004. Carbon cycling at ancient methane-seeps. *Chemical Geology,* 205, 443-467.

Peckmann, J., Thiel, V., Reitner, J., Taviani, M., Aarón, P. and Michaelis, W. 2004. A microbial mat of a large sulphur bacterium preserved in a Miocene methane-seep limestone. *Geomicrobiology Journal,* 21, 247-255.

Pin, C. and Bassin, C. 1992. Evaluation of a strontium-specific extraction chromatographic method for isotopic analysis in geological materials. *Analytica Chimica Acta*, 269, 249-255.

Ritger, S., Carson, B. and Suess, E. 1987. Methane-derived authigenic carbonates formed by subduction-induced pore-water expulsion along the Oregon/Washington margin. *Geological Society of America Bulletin*, 98, 147-156.

Rosenbaum, J. and Sheppard, S.M.1986. An isotopic study of siderites, dolomites and ankerites at high temperatures. *Geochimica et Cosmochimica Acta*, 50, 1147-1150.

Sartori, R., Torelli, L., Zitellini, N., Peis, D. and Lodolo, E. 1994. Eastern segment of the Azores-Gibraltar line (central-eastern Atlantic): An oceanic plate boundary with diffuse compressional deformation.*Geology*, 22, 555 - 558.

Savard, M.M., Beauchamp, B. and Veizer, J. 1996. Significance of aragonite cements around cretaceous marine methane seep. *Journal of Sedimentary Research*, 66, 430-438.

Schoell, M., 1980. The hydrogen and carbon isotopic composition of methanefrom natural gases of various origins. *Geochimica et Cosmochimica Acta,* 44, 649-661.

Shapiro, R. S. 2004. Recognition of fossil prokaryotes in Cretaceous methane seep carbonates: relevance to astrobiology. *Astrobiology*, 4, 438-449.

Shapiro, R. and Fricke, H. 2002. *Tepee Buttes: fossilized methane-seep ecosystems: Field Trip Guidebook*. Geological Society of America, Boulder, Colorado, 94-101.

Somoza, L. Díaz-delRío, V., León, R., Ivanov, M., Fernández-Puga, M. C., Gardner, J. M., Hernández-Molina, F. J., Pinherio, I. M., Rodero, J., Lobato, A., Maestro, A., Vázquez, J. T., Medialdea, T. and Fernández-Salas, L. M. 2003. Seabed morphology and hydrocarbon seepage in the Gulf of Cadiz mud volcano area: Acoustic imagery, multibean and ultra- high resolution seismic data. *Marine Geology,* 195, 153-175.

Stadnitskaia, A., Ivanov, M. K., Blinova, V., Kreulen, R. and van Weering, T. C. E. 2006. Molecular and carbon isotopic variability of hydrocarbon gases from mud volcanoes in the Gulf of Cadiz, NE Atlantic. *Marine Petroleum Geology*, 23, 281-296.

Stadnitskaia, A., Ivanov, van Weering, T.C.E., Sinninghe Damste. J.S., Werne, J.P., Kreulen, R. and Blinova, V. 2007. Molecular and isotopic characterization of hydrocarbon gas and organic matter from mud volcanoes of the Gulf of Cadiz, NE Atlantic. *IOC Workshop Report,* 175, 47.

Stadnitskaia, A., Ivanov, M.K., Poludetkina, E.N., Kreulen, R. and van Weering, T.C.E. 2008. Sources of hydrocarbon gases in mud volcanoes from the Sorokin Trough, NE Black Sea, based on molecular and carbon isotopic compositions. *Marine and Petroleum Geology*, 25, 1040-1057.

Steiger, R.H. and Jäger, E. 1977. Subcommission on geochronology: Convention on the use of decay constants in geoand cosmochronology. *Earth and Planetary Science Letters*, 36(3), 359-362.

Suess, E., Torres, M.E., Bohrmann, G., Collier, R.W., Greinert, J., Linke, P., Rehder, G., Trehu, A., Wallmann, K., Winckler, G. and Zuleger, E. 1999. Gas hydrate destabilization: enhanced dewatering, benthic material turnover and large methane plumes at the Cascadia convergent margin. *Earth and Planetary Science Letters*, 170, 1-15.

Teichert, B.M.A., Bohrmann, G. and Suess, E. 2005. Chemoherms on Hydrate Ridge-Unique microbially-mediated carbonate build-ups growing into the water column. *Palaeogeography, Palaeoclimatology, Palaeoecology*, 227, 67-85.

Terzi, C., Aharon, P., Ricci Lucchi, F. and Vai, G.B. 1994. Petrography and stable isotope aspects of cold-vent activity imprinted on Miocene-age bcalcaria Lucina Q from Tuscan and RomagnaApennines, Italy. *Geo-Marine Letters*, 14, 177-184.

Thiel, V., Peckmann, J., Seifert, R., Wehrung, P., Reitner, J. and Michaelis, W. 1999.Highly isotopically depleted isoprenoids: Molecular markers for ancient methane venting. *Geochimica et Cosmochimica Acta*, 63, 3959-3966.

Torelli, I., Sartori, R. and Zitellini, N. 1997. The giant chaotic body in the Atlantic Ocean off Gibraltar: new results from a deep seismic reflection survey. *Marine and Petroleum Geology*, 14 (2), 125-138.

Tortella, D., Torné, M. and Pérez-Estaún, A. 1997. Geodynamic Evolution of the Eastern Segment of the Azores-Gibraltar Zone: the Gorringe Bank and the Gulf of Cadiz Region. *Marine Geophysical Research*, 19, 211-230.

Vanneste, H., Kastner, M., James, R. H., Connelly, D, P., Fisher, R, E., Kelly-Gerreyn, B, A, Heeschen, K., Haeckel, M. and Mills, R, A. 2012. Authigenic carbonates from Darwin Mud Volcano, Gulf of Cadiz: A record of paleoseepage of hydrocarbon bearing fluids. *Chemical Geology*, 300-301, 24-39.

van Rensbergen, P., Depreiter, D., Pannemans, B., Moerkerke, G., van Rooij, D., Marsset, B., Akhmanov, G., Blinova, V., Ivanov, M., Rachidi, M., Magalhães, V., Pinheiro, L., Cunha, M. and Henriet, J. P. 2005. The El Arraiche mud volcano field at the Moroccan Atlantic slope, Gulf of Cadiz. *Marine Geology*, 219, 1-17.

Whiticar, M.J. 1999. Carbon and hydrogen isotope systematics of bacterial formationand oxidation of methane. *Chemical Geology,* 161, 291-314.

Wilkin, R.T. and Barnes, H.L. 1997. Formation processes of framboidal pyrite. *Geochimica et Cosmochimica Acta*, 61 (2), 323-339.

Recibido: febrero 2014
Revisado: septiembre 2014
Aceptado: noviembre 2014
Publicado: junio 2015